國立交通大學

電子物理系

碩士論文

矽奈米元件量子修正理論暨模式應用比較之研究

Modeling of Quantum Mechanical Effects for Nanoscale MOS Devices with Correction Theory

研究生：陳煒昕

指導教授：趙天生　博士

中華民國 九十五 年七月

E
S
A
1896

矽奈米元件量子修正理論暨模式應用比較之研究

Modeling of Quantum Mechanical Effects for Nanoscale MOS Devices with Correction Theory

研究生：陳煒昕	Student：Wei-Hsin Chen
指導教授：趙天生 博士	Advisor：Dr. Tien-Sheng Chao

國立交通大學
電子物理研究所
碩士論文

A Thesis
Submitted to Institute of Eletrophysics
College of Science
National Chiao Tung University
in partial Fulfillment of the Requirements
for the Degree of
Master
in

Electrophysics

July 2006

Hsinchu, Taiwan

中華民國九十五年七月


E
S
A
1896

E
S
A
1896

矽奈米元件量子修正理論暨模式應用比較之研究

學生：陳煒昕　　　　　　　　　　指導教授：趙天生 博士

國立交通大學 電子物理 學系（研究所）碩士班

摘　　要

隨著摩爾定律的趨勢，快速省電的要求，積體電路上的晶片將逐年縮小，現今工業界所量產的65奈米製程技術所製作的金氧半場效電晶體其閘極長度已接近次45奈米世代的試產進程，其中閘極氧化層厚度趨近1奈米。因此不同程度的量子效應已變顯著，半導體傳輸模式必須考慮此問題，量子修正的研究有助於電晶體的分析。

本論文完整介紹隱形式與顯形式的量子修正模式，其中顯形式模式包含Van Dort’s、Hänsch’s、Li’s、修正的局部密度趨近與有效位勢模式；隱形式模式分析了密度梯度方程式、修正的密度梯度方程式與熱力學有效位勢模式。論文中從理論推演以及數值分析方面仔細比較這些模式的優劣之處。量子修正模式中電子有效質量通常視為可調的數學參數，找出在不同的外加條件下所需要代入的數值對於半導體工業應用非常有利，尤其是顯形式模式更於容易使用。在應用上來說，吾人利用量子修正模式研究一維金氧半結構的電容特性以及考慮二維效應所影響的電流電壓關係式。

總之，本論文已從理論暨數值方向分析不同量子修正方法論的物理模式暨在金氧半場效電晶體應用之準確性。

Modeling of Quantum Mechanical Effects for Nanoscale MOS Devices with Correction Theory

Student：Wei-Hsin Chen　　Advisors：Dr. Tien-Sheng Chao

Department of Electrophysics
National Chiao Tung University

ABSTRACT

By the Moore's Law, chips manufactured on a wafer have approached sub-45 nm regime of gate length for metal-oxide-semiconductor-field-effect-transistors (MOSFETs). Quantum mechanics effects become significant and inevitable. Thus, the transport models used in semiconductors should be corrected by quantum correction models. In this thesis, explicit and implicit quantum correction models are introduced and reviewed completely. There are Van Dort's, Hänsch's, Li’s, modified local density approximation and effective potential models in explicit forms; density-gradient, modified density-gradient, thermodynamic effective potential models are in implicit forms. We compare these models with each other in terms of theoretical and numerical ways respectively. To find the relationship between the effective mass which is treated as fitting parameters in the models with varied physical settings is benefit for industry applications, especially the explicit models, they are simple to be implanted in the simulator. In application, C-V characteristics of a MOS structure and IV curves of a 20 nm double-gate MOSFET are numerically investigated in the work.


E
S
A
1896

誌謝

本論文得以順利完成，首先要感謝電物系 趙天生教授給予學生最大的自由度，讓學生得以進行感興趣的研究。學生感謝恩師，電信系　李義明副教授兩年來悉心指導；感謝老師們於碩士班受業期間對學生論文研究之激勵，思緒慎密之牽引以及觀念之啟迪。感謝李老師對於學生論文架構之匡正，研究方法傳授及用字遣辭之推敲斟酌。更銘誌於心的是恩師在為學處世及待人接物之諄諄教誨，使學生在治學方法及處世態度上受益良多，而恩師在學術研究之嚴謹精神，在半導體元件物理及電腦模擬領域之專業知識與生活處世的積極與認真的態度，更足以為學生日後之表率。師恩細長，深切銘心，學生在此謹獻上最誠摯的感謝與敬意。

論文口試期間，承蒙交通大學電子工程系陳明哲教授及交通大學電子物理系陳永富教授撥冗細審，並惠予寶貴意見與殷切指正使本論文更臻完備。

學生特別感謝台積電前瞻技術部經理楊富量博士給予學生機會，透過李老師與台積電的研究合作案，讓學生於碩士班二年級時至台積電工讀，學習理論與實務的結合，這難得的經驗奠定學生對於半導體領域的認識，藉此機會表達對於楊經理富量博士暨台積電的感謝。

感謝紹銘、正凱、宏穆、傳盛、彥羽、璞學長的照顧幫忙，同窗好友景嵐、柏賢、建松及婉文的互相砥礪，朝夕相伴，在此一併致謝。

受業期間，承蒙張國明老師、徐琅老師、陳永富老師、謝太炯老師、楊賜麟老師、陳振芳老師在學業上的悉心指導，在此一併感謝。

學生能順利完成研究所學業，全靠父母、家人及諸位朋友、同學的支持與忍耐，學生對此由衷感謝。

本論文感謝行政院國家科學委員會(計畫編號 NSC-93-2115-E-492-008、NSC-94-2115-E-009-084)、卓越延續計畫(計畫編號 NSC-94-2752-E-009-003-PAE、NSC-95-2752-E-009-003-PAE)、五年五百億計畫、經濟部科專計劃(計畫編號 93-EC-17-A-07-S1-0011)及台灣積體電路製造股份有限公司 2005~2006 年研究計畫之資助。

謹在此將本論文獻給關心我的人！

陳煒昕　謹誌

中華民國九十五年七月三十一日 于風城交大

E
S
A
1896

Acknowledgments (in English)

I would like to thank Professor Dr. Tien-Shang Chao of Department of Electrophysics and Professor Dr. Yiming Li of Department of Communication Engineering in National Chiao-Tung University. This thesis would not have been possible without their help and support. Professor Chao give me the whole freedom in pursuing this topic. I want to thank Professor Li for the courses I have taken with him and through the many discussions that we have had together.

In addition, I would like to express my appreciation to the members of my examination committee Professor Dr. Ming-Jer Chen and Professor Dr. Yung-Fu Chen for taking the time to read this thesis.

In the second year of my master program, though the project of Prof. Dr. Yiming Li, Manager Dr. Fu-Liang Yang gave me a very good opportunity to be an intern at department ETD 2 of TSMC. I am grateful to Manager Dr. Fu-Liang Yang and TSMC for the special experience in exploring semiconductor theory and manufacturing process.

I would also like to thank to all my friends, colleagues, and classmates especially Shao-Ming Yu, Cheng-Kai Chen, Hong-Mu Chou, Chuan-Sheng Wang, Pu Chen, Ching-Lan Chang, Bo-Shian Lee, Chien-Sung Lu and Wan Wen Lo.

I want to thank to the faculty members of National Chiao-Tung University, where I received the education after senior high school. I am lucky to have had the opportunity to learn from so many excellent instructors.

I further wish to acknowledge the financial support by Taiwan National Science Council (NSC) under constract NSC-93-2115-E-492-008, NSC-94-2752-E-009-003-PAE, NSC-94-2115-E-492-008 and NSC-95-2752-E-009-003-PAE, by the MOE ATU program under a 2006 grant, by the ministry of Economic Affairs, Taiwan, under contract 93-EC-17-A-07-S1-0011 and by the Taiwan Semiconductor Manufacturing Company under a 2004-2006 grant.

Last but not least, I would like to dedicate this thesis to my parents and family for their support and everlasting love and many others where space and time limits further mention of them, who have enriched my life by letting me take a peek through their eyeglass on the world.

Contents

Appendix A

List of Figures

Chapter 1

Introduction

The semiconductor industries have been the major part of today's technology development. With the prediction of Moore's Law, for the purpose of getting better electrical properties of transistors and a lower costs of very-large-scale integration (VLSI), device scaling is necessary and essential for semiconductor devices in the wafer, especially, metal-oxide-semiconductor field effect transistors (MOSFETs). There are many ways to study electrical characteristics of semiconductor devices. Besides measuring the electrical properties of manufactured chips on wafers in laboratory, there is still another quick and benefit way to analyze semiconductor devices, i.e., simulation and modelling. Simulation of semiconductors is divided into several kinds of ranks, as shown in Fig. 1.1. Many small units of device construct together to be a circuit, and then many circuits make a system. In this thesis, we concentrate on the device simulation. Simulation with good enough models and computation algorithms will give us precise predictions and trend of the physical features, without tremendous cost of fabrication process and save a lot of time simultaneously. Cost and time are the two most important issues if the industries can win in present keen competitions. Therefore, device simulation plays an important role in semiconductor industries. By the scaling of a semiconductor device, quantum mechanical effects become significantly influence on the performance of transistors. Thus, models introduced in simulation must consider quantum effects to obtain a correct predictions. Schr$\ddot{o}$dinger coupled Poisson's equations describes the electron behavior as a wave and particle duality and can predict the electrical properties very well compared with experiment data. However, it is time-consuming and difficult to solve in the point of view of numerical methods. Therefore, semi-classical equations with quantum correction models are wildly studied to substitute for Schr$\ddot{o}$dinger Equation. The semi-classical models have the most important purposes of speed and accuracy. In the thesis, effective quantum models are studied and compared with each other for nowadays advanced transistors.

This chapter is organized as follows. First of all, the motivation of this work is introduced, then a literature review of quantum correction models in semiconductor device is seated. Finally, outline of the thesis is described in detail.

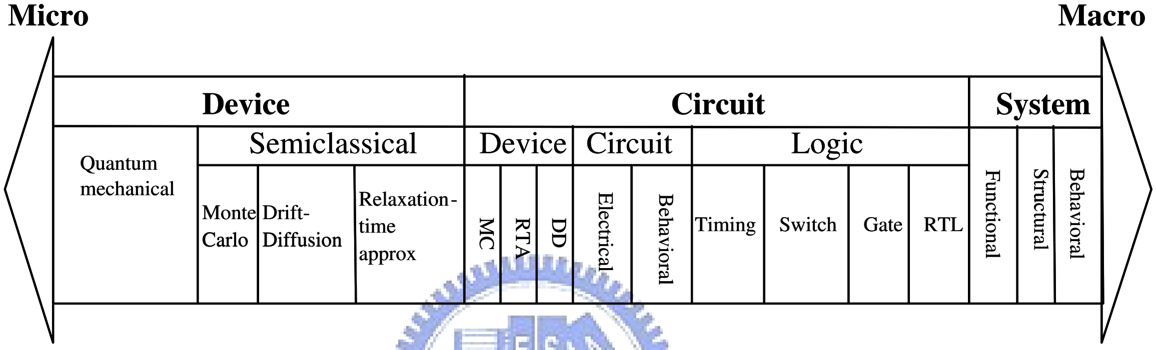

Figure 1.1: Hierarchy of semiconductor device simulation. Many small units of device construct together to be a circuit, and then many circuits make a system.

1.1 Motivation

With the continuous scaling down of the semiconductor devices. For example, gate oxide thickness less than 1 nanometer (nm) results in a large electric field in the interface between oxide and silicon and make the quantum well deep and narrow. The energy of electron wave functions in the inversion layer are quantized and limit the transport of electrons from source to drain. Therefore, the classical transport and other physical models are not accurate enough to obtain correct simulation results. Replacing the classical models by quantum ones are indispensable to consider the quantum effects, which are significant in today's nanoscale semiconductor devices. Nevertheless, it takes much time for a general computer in a lab when dealing with full quantum model, for example, the Schr$\ddot{o}$dinger equation, and therefore loses the benefit of fast speed. Simulation with classical models but importing an effective quantum term to approximate fully considered quantum models can keep the merits of fast and accuracy. However, the approximations of quantum effect proposed previously will lead to results which are not accurate enough or introduce some mathematical parameters which have no physical meanings. How to choose between accuracy and speed when using quantum correction models is what we concern about. In the thesis, we compare these quantum correction models in the point of view of theory and numerical simulation.

1.2 Literature Review

The importance of quantum effects in inversion layers of MOSFETs was recognized in the late 1950s by Schrieffer [1]. The initial research of quantum mechanical confinement in inversion layers was by Stern and Howard [2]. Later, Stern calculated energy levels, charge distribution, and electrostatic potential self-consistently in inverted p-type semiconductors [3]. Since the oxide thickness is continually reduced in order to maintain good control of the gate in nano-scale channel length regime, quantum mechanics become more significant. And a number of additional theoretical studies have been undertaken, such as Van Dort's model [4], the density-gradient approach [5], the modified local density approximation method, and the effective potential method [6]-[10]. Specifically, in the late 1980's, Hansch studies carrier transport at the interface between gate oxide and semiconductor, then developed a formula that allows an approximate incorporation of quantum mechanical boundary effects on the carrier distribution [11]. In the early 1990's, Van Dort used a simple method to model the silicon bandgap under the inversion condition [4]. He treated the quantum effects associated with the confinement of minority carriers in the inversion layer [12]. Although his model can predict the capacitance for a wide range of different doping levels, it fails to describe the quantum effect on the spatial distribution of electrons near the boundary layer, i.e. the pick value of electron distribution will away from the interface od Si/SiO_2. The density-gradient method is another approximation quantum treatment.It is a macroscopic approach to the quantum confinement problem. In the early 1980's, M. G. Ancona and H. F. Tiersten generalized the equation of describing the electron gas state to include density-gradient dependence [13]-[15]. Later it was extended to characterize the quantum- mechanical behavior of electrons distributed in strong inversion layers. Recently, Ancona and coworkers made further progress on this physically based approach and pointed out that the density-gradient approximation is an effective tool for engineering-oriented analysis of electronic devices in which quantum confinement and tunnelling phenomena are obvious [16]. The modified local density approximation (MLDA) approach was first used by Paasch and H. Ubensee in 1982 [17]. Using this method, they studied the electron density in an inversion layer in the semiconductor-insulator interface, which is approached with a triangular potential. Recently, an IBM semiconductor device simulation group developed a computationally efficient algorithm based on the MLDA. This model predicts the spatial distribution of the quantized carriers which the previously proposed simple models failed to do so. In the recent years, a effective potential (EP) approach has been proposed, which has the advantages of easy numerical implementation and almost guaranteed convergence [18][19]. The effective conduction-band edge equation which wants to improve the problem for density-gradient equation of a differential of a high order electron density is introduced [20]. In 2003, an improved Van Dort model is proposed, which is more to the results of Schrödinger-Poisson Equations. However, the fitting parameters have to be extracted by the optimization theory [21]. And then, a thermodynamic effective potential removes the disadvantage that fitting parameter has to be modified in different physical setting in Ferry's effective potential theory. Alternatively, the size of an electron is decided by its energy [22].

1.3 Outline

Physical models in semiconductor are shown in Chap. 2 and then basic descriptions of explicit and implicit quantum mechanical approximation models in Chap. 3 and Chap. 4, the new quantum potential correction models are investigated there. In Chap. 5, the application and comparison for MOS Structures by quantum correction models are displayed. Chap. 6 includes a summary of this work and suggestion for possible future work.

Chapter 2

Physical Models in Semiconductor

The electrical properties in semiconductor devices are the most important factors when judging if they are suitable for the applications, for example, high frequency or microwave devices. The main concepts of semiconductor device simulation have two components [23], which must be solved self-consistently with each other, i.e. the transport equations governing charge flow and the fields driving charge flow, as shown in Fig. 2.1. We can calculate the effective mass of electrons and potential between lattice. The data is loaded into the transport equation and then the electromagnetic field will upgrade current and charge density until the transport equation and electromagnetic field are solved consistently. After that, density, velocity and temperature of carriers, potential, electric field, I-V curve and C-V curve can be extracted [23]. To include the quantum mechanics, the

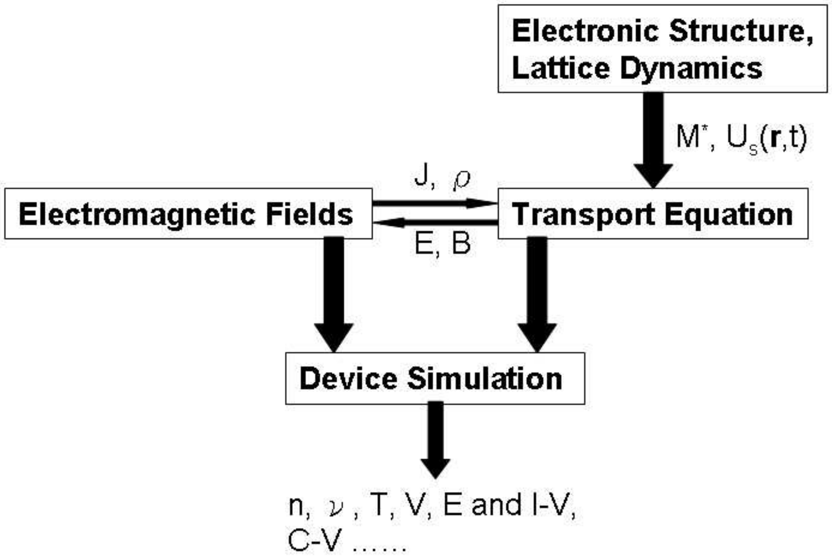

Figure 2.1: A schematic description of the device simulation sequence. The effective mass of electrons and potential between lattice are calculated. The data is loaded into the transport equation and then the electromagnetic field will upgrade current and charge density until the transport equation and electromagnetic field are solved consistently. After that, density, velocity and temperature of carriers, potential, electric field, I-V curve and C-V curve can be extracted.

direct solution of many-body time-dependant Schrödinger equations are only suitable for few number of particles, so it's not a possible way to be used in semiconductor. Alternatively, approximation methods are often adopted for simulation, as shown in Fig. 2.2. The arrows in the bottom mean more accurate but costs more time; the upper ones mean more approximate, fast and easy. The selection of models depends on the compromise between accuracy and speed. These models are described in detail in the next sections.

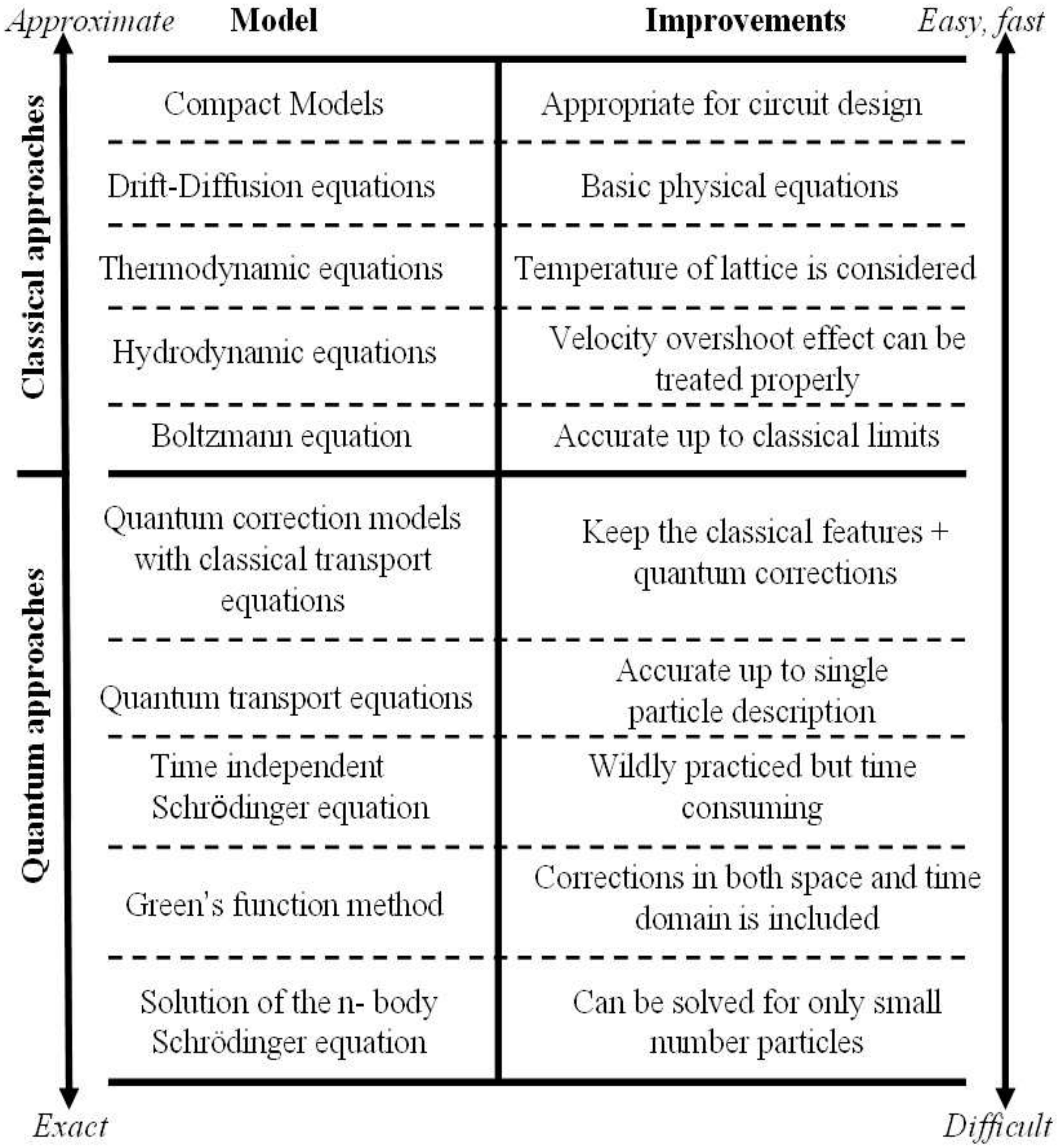

	Model	Improvements
Classical approaches	Compact Models	Appropriate for circuit design
	Drift-Diffusion equations	Basic physical equations
	Thermodynamic equations	Temperature of lattice is considered
	Hydrodynamic equations	Velocity overshoot effect can be treated properly
	Boltzmann equation	Accurate up to classical limits
Quantum approaches	Quantum correction models with classical transport equations	Keep the classical features + quantum corrections
	Quantum transport equations	Accurate up to single particle description
	Time independent Schrödinger equation	Wildly practiced but time consuming
	Green's function method	Corrections in both space and time domain is included
	Solution of the n- body Schrödinger equation	Can be solved for only small number particles

Figure 2.2: Illustration of a hierarchy of various transport models.The arrows in the bottom mean more accurate but costs more time; the upper ones mean more approximate, fast in simulation and easy to implantation.

2.1 Maxwell's Equations

The fields for the charge and current density are obtained from solving Maxwell's equations [24][25]

$$\begin{aligned} \nabla \times \vec{H} &= \vec{J} + \frac{\partial \vec{D}}{\partial t}, && (2.1) \\ \nabla \times \vec{E} &= -\frac{\partial \vec{B}}{\partial t}, && (2.2) \\ \nabla \cdot \vec{D} &= \rho, && (2.3) \end{aligned}$$

and

$$\nabla \cdot \vec{B} = 0, \qquad (2.4)$$

where $\vec{E}$ and $\vec{D}$ are the electric field and displacement vector. $\vec{H}$ and $\vec{B}$ are the magnetic field and induction vector. $\vec{J}$ denotes the conduction current density and ρ is the electric charge density. Under appropriate conditions [26], only the quasi-static electric fields arising from the solutions of Poisson's equation are necessary. Poisson's equation is essentially derived from $\nabla \cdot \vec{D} = \rho$. By substituted for some basic physical formulas, given by

$$\begin{aligned} \vec{D} &= \varepsilon \cdot \vec{E}, && (2.5) \\ \vec{E} &= -\nabla V, && (2.6) \end{aligned}$$

and

$$\rho \quad = \quad q(p - n + N_A^+ - N_D^-), \tag{2.7}$$

where ε is the permittivity tensor and V is the potential. q denotes the electron charge. p, n, N_A^+ and N_D^- are densities of hole, electron, ionized acceptors and ionized donors, respectively. Then a Poisson's equation has the form of

$$\nabla \cdot V = \frac{q}{\varepsilon}(n - p + N_D^- - N_A^+). \tag{2.8}$$

The continuity equation can be derived from Maxwell's equation or Boltzmann equation. In this section, deviation form $\nabla \times \vec{H} = \vec{J} + \frac{\partial \vec{D}}{\partial t}$ by $\vec{J} = \vec{J}_p + \vec{J}_n$ with assumptions of unchanged donors and acceptors with respect to time is shown as

$$\nabla \cdot (\vec{J}_p + \vec{J}_n) + q \cdot \frac{\partial}{\partial t}(p - n) = 0. \tag{2.9}$$

Considering the generation and recombination term, R, and then Eq. (2.9) becomes

$$\nabla \cdot (\vec{J}_n) - q \cdot \frac{\partial n}{\partial t} \quad = \quad q \cdot R, \tag{2.10}$$

and

$$\nabla \cdot (\vec{J}_p) + q \cdot \frac{\partial p}{\partial t} \quad = \quad -q \cdot R, \tag{2.11}$$

in terms of electron and hole respectively.

2.2 Classical Transport Models in Semiconductor Device

In the numerical analysis, the current are characterized by either classical or quantum transport equations. Before the gate lengths of MOSFETs are scaled down to less than 100 nm by the rule of Moore's Law [27], the transport properties is sufficient to be described by classical transport equations. Semiconductor equations, derived from the Boltzmann transport equation, are the basis of the majority of current device models, where the dimensions of the device geometry are greater than a de Broglie wavelength of electrons. The classical transport equations are introduced in the next sections.

The transport equation used in semiconductor in classical regime is based on Boltzmann equation and its simplified models, i.e. hydrodynamic, thermodynamic and drift-diffusion models.

2.2.1 Boltzmann Equation

The Boltzmann transport equation describes the temporal evolution of the single-particle distribution function $f(r,p,t)$ in the phase space [28]. The coordinates of particles in space, r, and momentum, p, at a certain time can be characterized well. Assume there are scattering effects , the distribution function is given by [28]

$$\frac{df(r,p,t)}{dt} = \frac{\partial f}{\partial t}_{collision}, \tag{2.12}$$

which expands to yield [26],

$$\frac{\partial f}{\partial t} + \frac{\partial r}{\partial t} \cdot \nabla_r f + \frac{\partial p}{\partial t} \cdot \nabla_p f = \frac{\partial f}{\partial t}_{collision}. \tag{2.13}$$

The rate of change of momentum $\frac{\partial \vec{p}}{\partial t}$ is equal to the applied force $F = q\vec{E}(\vec{r},t)$ and $\frac{\partial \vec{r}}{\partial t}$ is equal to the group velocity, $\vec{u}(\vec{k})$. $\vec{p}$ is substituted by $\vec{k}\hbar$. Then Eq. (2.12) can be written as

$$\frac{\partial f(\vec{r},\vec{k},t)}{\partial t} + \vec{u}(k) \cdot \nabla_r f(\vec{r},\vec{k},t) + \frac{-q\vec{E}(\vec{r},t)}{\hbar} \cdot \nabla_k f(\vec{r},\vec{k},t) = \frac{\partial f \vec{r},\vec{k},t}{\partial t}_{collision}. \tag{2.14}$$

In Boltzmann equation, carriers are treated as classical particles which are uncorrelated with position $\vec{r}$ and momentum $\vec{k}$ at time t. A many-particle system of carriers and be expressed as single-particle distribution [29].

The Boltzmann euqation is the most accurate in the classical limit and a statistical Monte Carlo method is used to find the distribution function. However, it consumes the computation a lot. Therefore, some simplified equations, for example, hydrodynamic equations, are adopted to replace Boltzmann equation for the purpose of compromise between accuracy and simulation time. Before preforming the deviation, some equations are defined as follows, $n(\vec{r},t)$ is the electron concentration:

$$n(\vec{r},t) = \int_{-\infty}^{\infty} f(\vec{r},\vec{k},t)d\vec{k}; \tag{2.15}$$

$v_{dn}(\vec{r},t)$ is the electron average velocity;

$$n(\vec{r},t)v_{dn}((\vec{r},t)) = \int_{-\infty}^{\infty} \vec{u}(\vec{k})f(\vec{r},\vec{k},t)d\vec{k}; \tag{2.16}$$

$\omega_n(\vec{r},t)$ is the electron average energy:

$$n(\vec{r},t)\omega_n((\vec{r},t)) = \frac{m_n^*}{2}\int_{-\infty}^{\infty} |\vec{u}(\vec{k})|^2 f(\vec{r},\vec{k},t)d\vec{k}; \tag{2.17}$$

$\vec{T}_n(\vec{r},t)$ is the electron temperature tensor:

$$\frac{1}{2}n(\vec{r},t)k_B\vec{T}_n((\vec{r},t)) = \frac{m_n^*}{2}\int_{-\infty}^{\infty}[\vec{u}(\vec{k}) - v_{dn}(\vec{r},t)]f(\vec{r},\vec{k},t)d\vec{k}; \quad \texttt{and} \tag{2.18}$$

$\vec{Q}_n(\vec{r},t)$ is the heat flow vector:

$$\vec{Q}_n((\vec{r},t)) = \frac{m_n^*}{2}\int_{-\infty}^{\infty}[\vec{u}(\vec{k}) - v_{dn}(\vec{r},t)]|\vec{u}(\vec{k}) - v_{dn}(\vec{r},t)|^2 f(\vec{r},\vec{k},t)d\vec{k}. \tag{2.19}$$

2.2.2 Hydrodynamic Equations

If we multiply a $\chi(\vec{k})$ in Eq. (2.14) and integrate from minus infinity to infinity, Eq. (2.14) becomes [30]

$$\begin{aligned}\int_{-\infty}^{\infty}\chi(\vec{k})\frac{\partial f(\vec{r},\vec{k},t)}{\partial t}d\vec{k} \quad &+ \quad \int_{-\infty}^{\infty}\chi(\vec{k})\vec{u}(k)\cdot\nabla_r f(\vec{r},\vec{k},t)d\vec{k} + \int_{-\infty}^{\infty}\chi(\vec{k})\frac{-q\vec{E}(\vec{r},t)}{\hbar} \\ \cdot\nabla_k f(\vec{r},\vec{k},t)d\vec{k} \quad &= \quad \int_{-\infty}^{\infty}\chi(\vec{k})\frac{\partial f\vec{r},\vec{k},t}{\partial t}_{collision}d\vec{k}.\end{aligned} \tag{2.20}$$

Then balance equations are decided through assumptions [30][31]. If $\chi(\vec{k})$ is defined as 1, i.e. the 0th order approximation, then Eq. (2.20) is derived to the carrier balance equation, given by

$$\frac{\partial n(\vec{r},t)}{\partial t} + \nabla_r (n(\vec{r},t)\vec{v}_{dn}(\vec{r},t)) = G(\vec{r},t) - R(\vec{r},t). \tag{2.21}$$

If $\chi(\vec{k})$ is defined as $m_n^* \vec{u}(\vec{k})$, i.e. the 1st order approximation, then Eq. (2.20) is derived to the momentum balance equation, given by

$$\begin{aligned} \frac{\partial (n(\vec{r},t)\vec{v}_{dn}(\vec{r},t))}{\partial t} + \nabla_r \cdot \frac{n(\vec{r},t)k_B\vec{T}_n(\vec{r},t)}{m_n^*} &+ \nabla_r \cdot (n(\vec{r},t)\vec{v}_{dn}(\vec{r},t)^2) + \frac{q\vec{E}}{m_n^*}n(\vec{r},t) \\ &= \left.\frac{\partial (n(\vec{r},t)v_{dn}(\vec{r},t))}{\partial t}\right|_{collision}. \end{aligned} \tag{2.22}$$

If $\chi(\vec{k})$ is defined as $\frac{1}{2}m_n^* \vec{u}(\vec{k})^2$, i.e. the 2nd order approximation, then Eq. (2.20) is derived to the energy balance equation, given by

$$\begin{aligned} \frac{\partial (n(\vec{r},t)\vec{\omega}_n(\vec{r},t))}{\partial t} &+ \nabla_r \cdot [\vec{v}_{dn}(\vec{r},t)n(\vec{r},t)\omega_n(\vec{r},t) + \vec{v}_{dn}(\vec{r},t) \cdot n(\vec{r},t)k_B\vec{T}_n(\vec{r},t) + \vec{Q}_n(\vec{r},t)] \\ &+ qn(\vec{r},t)\vec{v}_{dn}(\vec{r},t) \cdot \vec{E} = \left.\frac{\partial (n(\vec{r},t)\vec{\omega}_n(\vec{r},t))}{\partial t}\right|_{collision}. \end{aligned} \tag{2.23}$$

The hydrodynamic equations for electron is composed by these three parts shown above. Therefore, we need to solve seven partial differential equations for using the hydrodynamic model when considering electron, hole, and Poisson equations. The model can reproduce hot carrier effects as velocity overshoot and accurate impact ionization generation rates which drift-diffusion model lacks [32].

2.2.3 Energy Transport Equations

The energy transport equations only consider particle conservation, Eq. (2.21), and energy conservation, Eq. (2.23) [33], which lacks momentum conservation compared with hydrodynamic model. It accounts for electrothermal effects, under the assumption that charge carriers are in thermal equilibrium with the lattice [34]. Under approximations [35], particle conservation relation becomes:

$$\frac{\partial n}{\partial t} = \frac{1}{q}\nabla \cdot \vec{J}_n - R, \tag{2.24}$$

where $\vec{J}_n$ is the electron current density, shown as

$$\vec{J}_n = -q\mu_n n \nabla\phi + qD_n \nabla n + \mu_n k_B n \nabla T_n. \tag{2.25}$$

Energy balance equation becomes:

$$\frac{\partial (n\omega_n)}{\partial t} = -\nabla \cdot \vec{S}_n + \vec{J}_n \cdot \vec{E} - n\frac{\omega_n - \omega_0}{\tau_{n\omega}(T_n)}, \tag{2.26}$$

where $\vec{S}_n$ is the electron energy flux, shown as

$$\vec{S}_n = \frac{\vec{J}_n}{-q}\omega_n + \frac{\vec{J}_n}{-q}k_B T_n + \vec{Q}_n. \tag{2.27}$$

ω_n is the average carrier energy and $\vec{Q}_n$ is the heat flux, given by

$$\omega_n = \frac{3}{2}k_B T_n + \frac{1}{2}m_n^* v_{dn}^2, \tag{2.28}$$

and

$$\vec{Q}_n = -2T_n(\frac{k_B}{q})^2 nq\mu_n \nabla T_n. \tag{2.29}$$

Therefore, including electron, hole and Poisson equations, we have to solve five partial differential equations when considering energy transport equations.

2.2.4 Drift-Diffusion Equations

The drift-diffusion equations are widely used for the simulation of carrier transport in semiconductors by its simple and fast properties in simulation [36]. It should be considered carefully because some properties such as heat effects, are neglected in the model. We only use the carrier balance equation, Eq. (2.21), to have, for electron [36],

$$\frac{\partial n}{\partial t} = \frac{1}{q}\nabla \cdot \vec{J_n} - R, \tag{2.30}$$

where

$$\vec{J_n} = -q\mu_n n \nabla \phi + qD_n \nabla n. \tag{2.31}$$

Accordingly, only three partial differential equations need to be solved when considering electron, hole and Poisson's equations.

2.3 Quantum Approaches in Semiconductor Device

The sizes of MOSFETs fabricated on silicon substrate for VLSI have been scaled in order to attain better performance and higher integration. The gate length of a MOSFET (multi-gates) keeps shrinking even over 10 nm [37]. With the size reduction of the horizontal direction, i.e. direction from source to drain, the vertical direction such as gate oxide thickness and depletion layer thickness scale down at the same time to lead to a strong quantum confinement effects [38].

Accordingly, two significant quantum effects appear, for example, a shift in the threshold voltage due to a rise of the lowest occupied subband above the minimum conduction band energy and a reduction in the gate capacitance because of the setback of the maximum in the inverted electron density away from Si/SiO$_2$ interface. These quantized effects can be integrated into the classical models though some kinds of quantum approximation which has explicit or implicit forms. However, if the lateral quantization becomes important, then a full quantum mechanical model is required to deal with the device. In this section, a brief description for quantum approximations is given.

2.3.1 Time-independent Schrödinger Equation

The direct solution of many-body Schrödinger equation can be solved only for small number of particles, so it's not possible to be applied into the whole device simulation. Thus, we approximate the quantum effects into single-state and time-independent Schrödinger Equation and then coupled with the Poisson equation. Classical transport models are adopted when current calculation is needed. We consider a MOS structure, where the metal part is replaced by polycrystal silicon with a p-type silicon as substrate. Two assumptions are adopted [39]. The first, Fermi-Dirac distribution is employed and the second, standard electron and hole effective-mass approximations in a parabolic shaped band are assumed. Fig. 2.4 shows the energy band diagram of a MOS structure. The flow chart of the self-consistent Schrödinger and Poisson system is shown in Fig. 2.5 [40]. We must first give the initial guesses of potential and electron density to start the first iteration of self-consistent system. We can get a upgraded potential from Poisson equation, Eq. (2.8), and renew the potential term in Schrödinger equation simultaneously. The nest step is to solve Schrödinger equation, which is shown below,

$$-\frac{\hbar^2}{2m_{xk}}\frac{d^2}{dx^2}\zeta_{jk}(x)+E_C(x)\zeta_{jk}(x)=E_{jk}\zeta_{jk}(x), \tag{2.32}$$

where m_{xk} is the effective mass normal to the interface in the kth valley, E_{jk} is the energy levels of the jth subband in the kth valley, and ζ_{jk} is the wave function of the jth subband in the kth valley. A zero wave function boundary condition is used at the quantum system boundary. Because the silicon crystal has a six-folds ellipse-shape band energy diagram, there are two different effective mass (m_{jk}) when dealing with different kth valley. It should be chosen carefully.

After the Schr$\ddot{o}$dinger equation is solved, wave function and eigen-energy are known. And then charge density can be calculated.

Region 1, i.e. the silicon bulk region, where the electron energy is continuous and therefore all energy levels above the conduction band minimum edge (E_C) are permissible. Electron density in the classical region is calculated by [41]

$$n_{cl} = N_c e^{\gamma}[1 - c_1 e^{\gamma} + c_2 e^{2\gamma}]. \tag{2.33}$$

where,

$$\begin{aligned} \gamma(x) &= \frac{E_F - E_C(x)}{k_B T} = \frac{E_F - (-q\psi(x))}{k_B T}, \\ c_1 &= 0.3536, \end{aligned}$$

and

$$c_2 = 0.1290.$$

And electrons in the inversion region near the surface of Si/SiO$_2$ in silicon substrate (region 2) are treated as a two dimensional electron gas (2DEG) with a splitting of energy levels into subbands. Where the electrons are divided into two parts: (1) One of them is calculated as 2DEG where the potential is sufficiently narrow to quantize the motion in the inversion layer, and (2) the others whose energies are above E_{lim} behave like classical particles. As shown below,

$$n = n_q + n_{cl}. \tag{2.34}$$

If the first eight subbands are considered, n_q is given by [42]

$$n_q(x) = \frac{k_B T}{\pi \hbar^2} \sum_{k=1}^{2} g_k m_{dk} \sum_j \ln[\frac{1+\exp(\frac{E_F - E_{jk}}{k_B T})}{1+\exp(\frac{E_F - E_{lim}}{k_B T})}] |\zeta_{jk}|^2. \tag{2.35}$$

where, ζ_{jk} is the envelope function of the jth subband in the kth valley, g_k is the degeneracy factor of the kth valley, and m_{dk} is the parallel effective mass in the kth valley. And the electrons behave classically as

$$n_{cl}(x) = N_C \frac{2}{\sqrt{\pi}} \int_{\xi_0(x)}^{\infty} \frac{\sqrt{\xi} d\xi}{1+\exp \xi - \gamma(x)}, \tag{2.36}$$

where,

$$\xi_0(x) = \frac{E_{lim} - (-q\psi(x))}{k_B T}.$$

The hole has no quantum confinement and the density p can be calculated by the classical Boltzmann distribution,

$$p = N_V \exp(\frac{E_V(x) - E_F}{\kappa_B T}). \tag{2.37}$$

Therefore, the charge density in the inversion layer is calculated by

$$\rho = q(p - n + N_D^+ - N_A^-). \tag{2.38}$$

We get the new n_{cl} and n_q. If the system has not converge, the charge density term in Poisson equation is renovated again to begin the second time of iteration. The process carries on until convergence criterion is achieved. The total inversion layer charge $< Q >$ is obtained by the integration over electron density, which is defined as

$$< Q >= \int_0 n(r)dr, \tag{2.39}$$

where $n(r)$ is electron density. The average inversion charge depth $< X >$ is defined as

$$< X >= \frac{\int_0 rn(r)dr}{\int_0 n(r)dr}. \tag{2.40}$$

The Schr$\ddot{o}$dinger-Poisson system is the most accurate way of steady-state to treat the quantum confinement problems in the inversion layer at the Si/SiO$_2$ interface. But it has the fatal disadvantages of taking too much time and consuming the computer efficiency seriously when dealing with the eigen-value problems of Schr$\ddot{o}$dinger equations. However, the quantum effect is a very important phenomenon that can't be neglected in such small scale dimension of transistors. Therefore, not only for the applications of industries but also for the research of academics, the quantum approximation models (quantum correction models) are developed for the purpose of replacing the Schr$\ddot{o}$dinger equations by approximation of mathematical forms to get a much fast simulation speed and accurate enough results in the past years. In brief, these models have the explicit and implicit types and are summarized in the next chapters.

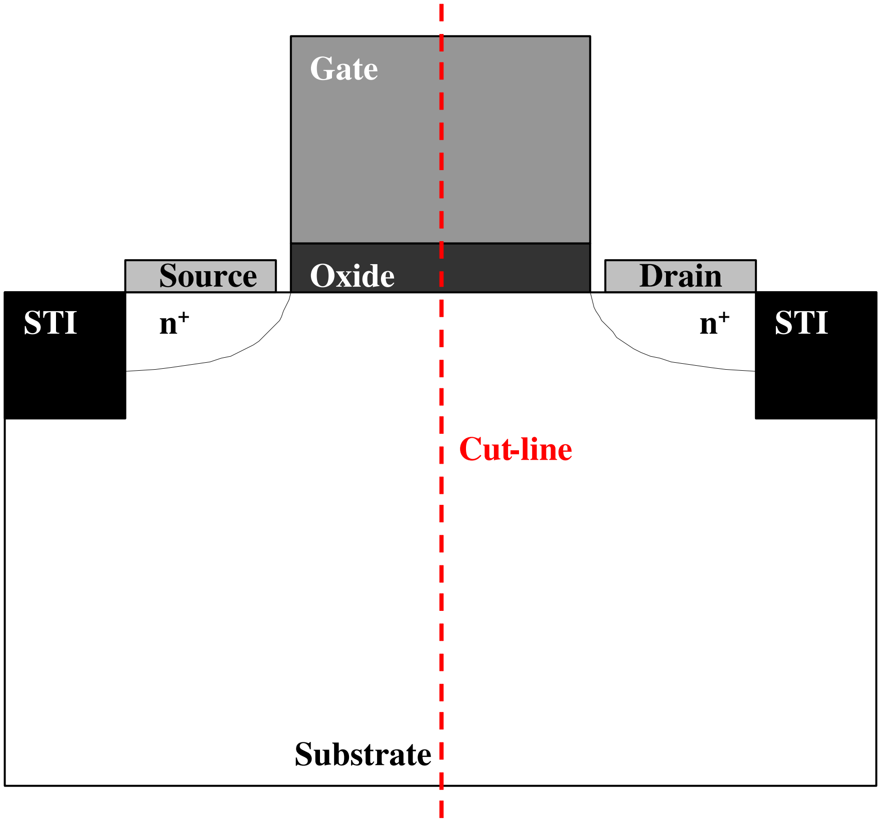

Figure 2.3: Single-gate MOS structure. We can draw the band diagram as Fig. 2.4. along the direction of red-dashed cut-line.

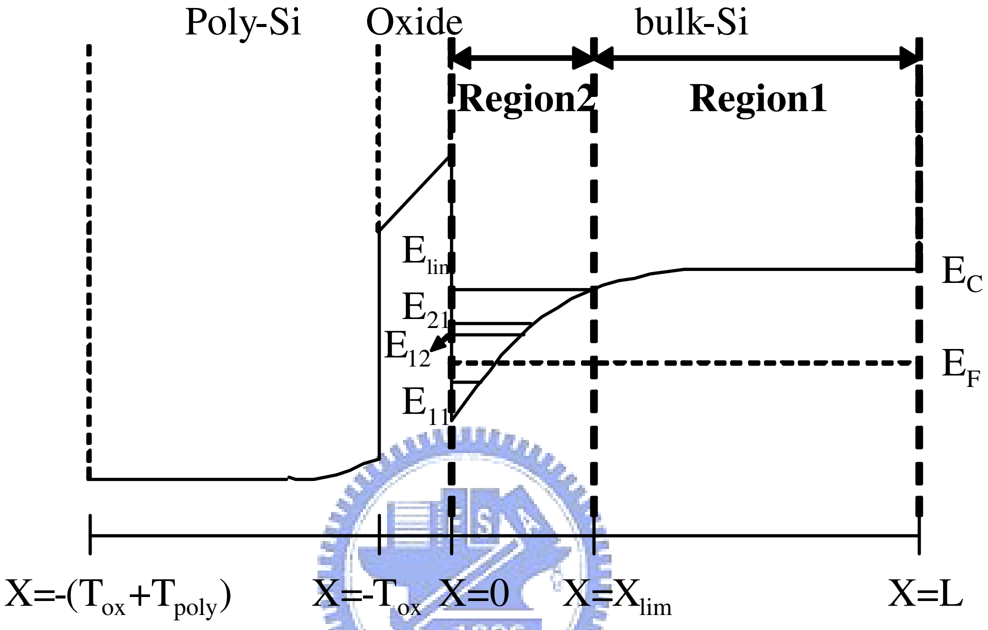

Figure 2.4: Energy band diagram of a MOS structure. T $_{ox}$ is oxide thickness, T $_{poly}$ is poly-silicon thickness, X$_{lim}$ corresponds to the eighth subband and L is the length od substrate; E$_{11}$ is the first subband, E$_{12}$ is the second subband, E$_{21}$ is the third subband and E$_{lim}$ is the eighth subband.

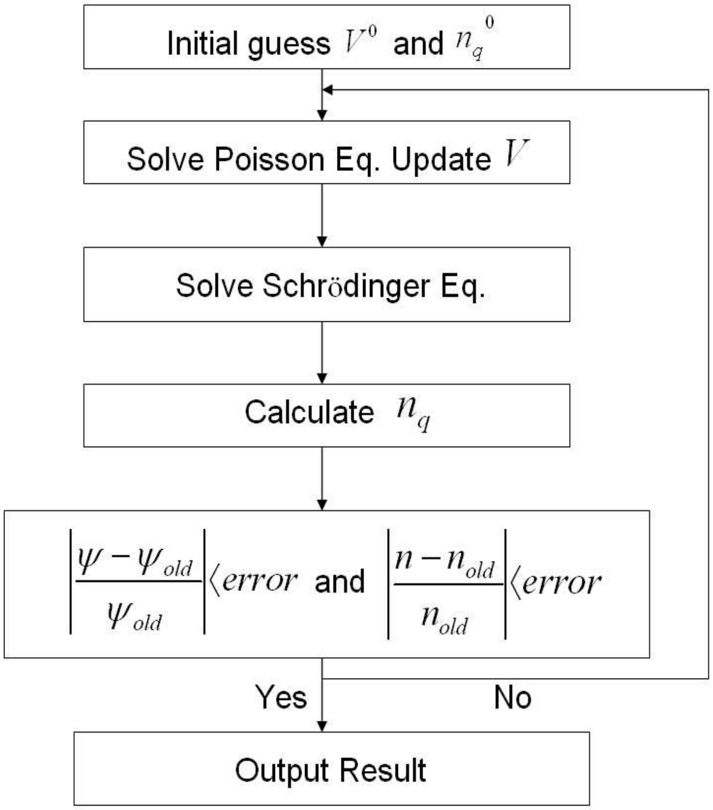

Figure 2.5: Schrodinger-Poisson flow chart. Give the initial guesses of potential and electron density first to start the first iteration of self-consistent system. Then the potential from Poisson equation is upgraded, and renew the potential term in Schrödinger equation simultaneously. If the stop criterion is reached, the self-consistent procedure is done, or the latest potential and electron density have to be upgraded again until the error is small enough [40].

2.3.2 Quantum Transport Theory

If a system containing a large number of particles is not completely known, we usually use the statistical physics of concept of statistical ensemble. Classical transport physics is based on the concept of probability distribution function which describe the phase space of carriers. However, in quantum mechanics, obtaining details about position and momentum simultaneously contradicts the Heisenberg's Uncertainty Principle. Therefore, it is given by a probability density matrix in terms of quantum mechanics. The rate of change of the probability density matrix ρ with time is determined by Lioville-von Neumann equation, given by [43][26]

$$i\hbar\frac{\partial\rho}{\partial t} = [H, \rho], \tag{2.41}$$

where the density matrix, ρ, is defined as

$$\rho = \sum_{i=0}^{\infty}\rho_i|\psi_i\rangle\langle\psi_i|. \tag{2.42}$$

This is the quantum analogue of the Liouville equation in classical transport equation, shown as

$$\begin{aligned} \frac{\partial\rho}{\partial t} &= \{H, \rho\}, \\ \Rightarrow\quad \frac{\partial\rho}{\partial t} &= \sum_{i=1}^{n}(\frac{\partial H}{\partial q_i}\frac{\partial\rho}{\partial p_i} - \frac{\partial\rho}{\partial q_i}\frac{\partial H}{\partial p_i}) \end{aligned} \tag{2.43}$$

There is another alternative approach. Draw an analogy to classical concept of a phase-space distribution function, the quantum mechanics use a Wigner distribution function. It is very similar to Boltzmann equation with the constraints of the uncertainty principle but has no simple interpretation in the concept of probability theory since it is not definitely positive definite. Wigner function extends the concept of distribution to the quantum case and it constitutes the more direct link between the quantum density matrix and the classical description of the evolution of the system in phase space though a distribution function $f(\vec{r}, \vec{p}, t)$, defined by [22]

$$f(\vec{r}, \vec{p}, t) = (2\pi)^{-3} \int_{R^3} \rho(\vec{r} + \frac{\hbar}{2}\eta, \vec{r} - \frac{\hbar}{2}\eta) exp(i\eta \cdot \vec{p}) d\eta. \tag{2.44}$$

By analogy with Boltzmann transport equation, the Wigner transport equation has a similar form, given by

$$\partial_t f + \frac{1}{m^*}\nabla_r \cdot (\vec{p}f) - e\theta[V]f = (\frac{\partial f}{\partial t})_{collision}, \tag{2.45}$$

where $\theta[V]$ is a pseudodifferentail operator, shown as

$$\theta[V] = \frac{i}{\hbar}[V(\vec{r} + \frac{\hbar}{2i}\nabla_p) - V(\vec{r} - \frac{\hbar}{2i}\nabla_p)]. \tag{2.46}$$

And the action of $\theta[V]$ is given by

$$\theta[V]f(\vec{r}, \vec{p}, t) = (2\pi)^{-3} \int_{R^3}\int_{R^3} \frac{i}{\hbar}[V(\vec{r} + \frac{\hbar}{2}\eta) - V(\vec{r} - \frac{\hbar}{2}\eta)] f(\vec{r}, \vec{q}, t) exp[i\eta \cdot (\vec{p} - \vec{q})] dq d\eta. \tag{2.47}$$

Quantum transport theory is used to explain and support confidence limits for the classical Boltzmann transport theory.

2.3.3 Quantum Correction Models

Without solving Schr$\ddot{o}$dinger equation and using the quantum transport theory, there is another way to consider quantum mechanical effects into device simulation. It is a semiclassical method to treat the quantum effects by replacing a classical potential by a corrected potential or a classical carrier concentration by corrected carrier one. This kind of quantum correction methods are not as accuracy as what has been discussed in the previous sections, they are compromises between precision and calculating time. Fast speed in simulation is the most beneficial in semiclassical transport equations with quantum correction models. It is easy to upgrade the potential or carrier concentration term in classical transport equations and there are two types of such quantum correction models, i.e. explicit and implicit models. They are introduced by detail in Chap. 3 and Chap. 4. In the commercial simulation tools, drift-diffusion transport equations with quantum corrected models are wildly adopted because of properties of simple and fast. Similarly, the hydrodynamic and Boltzmann equations can also transformed to semiclassical form by renewing the correction term. Which sort of transport models is chosen just depends on what physical phenomenons need to be considered in simulation process.

Chapter 3

Explicit Quantum Corrections

In the chapter, the explicit quantum corrections, i.e., the Van Dort's model, H$\ddot{a}$nsch model, Li's model, MLDA model and effective potential model, are discussed in terms of theoretical viewpoint.

3.1 The Van Dort's Model

The Van Dort's model considers the quantum effect at the interface of Si/SiO$_2$ as a effective rise of the minimum conduction band edge as a widened bandgap. The model proposes that the quantum corrected surface potential ψ_s^Q is larger than the conventional potential ψ_s^{conv} by [4]

$$\psi_s^Q = \psi_s^{conv} + \frac{\Delta E}{q} + \varepsilon_s \Delta\bar{x}, \tag{3.1}$$

where ΔE is the energy level difference between the minimum conduction band edge and the first allowed energy level E_{11} in the quantized region at the interface, ε_s is the surface electric field, and $\Delta\bar{x}$ is the difference of the average displacement of electrons from interface of Si/SiO$_2$ between classical and quantum solutions. If the bandgap is larger enough, we can approximate the quantum corrected intrinsic carrier concentration n_i^Q, which is shown as

$$\begin{aligned} n_i^Q &= n_i exp(\frac{E_F - \frac{E_g^Q}{2}}{k_B T}) \\ &= n_i exp(\frac{E_F - \frac{E_g}{2}}{k_B T}) exp(\frac{\triangle E_1}{2k_B T}) \\ &= n_i^{conv} \exp(\frac{E_g^Q - E_g^{conv}}{2k_B T}), \end{aligned} \tag{3.2}$$

where n_i^{conv} is the classical model for the intrinsic carrier concentration, E_g^Q is quantum corrected bandgap, and E_g^{conv} is the original bandgap. E_1 is the difference between E_g^Q and E_g^{conv}. Since the quantum effect is only significant near the interface, a weighting factor $W(x)$ can be introduced approximately as

$$W(x) = \frac{2\exp(-a^2)}{1 + \exp(-2a^2)}, \tag{3.3}$$

to model the potential distribution in the direction perpendicular to the interface of Si/SiO$_2$. Where $a = \frac{x}{x_{ref}}$ and x_{ref} is a reference distance ($x_{ref} \approx$ 25 nm). Thus, the upgraded and quantum corrected intrinsic carrier concentration n_i is given by

$$n_i = n_i^{conv}[1 - W(x)] + W(x) n_i^Q. \tag{3.4}$$

Although the Van Dort's Model has a simple mathematical form to implement to the classical solver, it has the drawbacks that it is not accurate because of triangular well approximation and it cannot predict the condition that the peak electron density value has a distance away from the Si/SiO$_2$ interface. The electron density will still has the largest value at the interface like the behavior of classical electrons. The method can only describe the decreasing electron density accounting for a reduced effective bandgap.

3.2 The H$\ddot{a}$nsch's Model

The H$\ddot{a}$nsch's Model approximates the electron concentration density with quantum correction as [11]

$$n^Q(x) = N_C \exp(-\frac{q\psi(x) - q\phi_F}{k_B T})[1 - \exp(-\frac{x^2}{\lambda_{th}^2})], \tag{3.5}$$

where λ_{th} is the thermal wavelength shown as

$$\begin{aligned} \lambda_{th} &= \sqrt{\frac{\hbar^2}{2m_n^* k_B T}}, \\ m_k &= \frac{m_n^*}{9.11 \times 10^{-31} kg}. \end{aligned} \tag{3.6}$$

λ_{th} is a measure of how fast the quantum effect decreases away from the interface, m_n^* is an effective electron mass, N_C is the conduction band effective density-of-states, $\phi_F = \frac{E_F}{q}$, and E_F is fermi level. This model is smoothed to have a classical electron density when the position is far away from the interface of Si/SiO$_2$, shown as

$$n^{classical}(x) = N_C \exp(-\frac{q\psi(x) - q\phi_F}{k_B T}). \tag{3.7}$$

It is a classical model of electron density which is corrected by an additional term, $1 - exp(-\frac{x^2}{\lambda_{th}^2})$. The electron concentration changes rapidly in the boundary layer (Si/SiO$_2$ interface), it is difficult to evaluate an accurate value from Poisson equation. Generally, we can assume the electron concentration is proportional to $(x - x_{interface})^2$ at interface and this assumption is valid for electron concentration for Hänsch's, modified local density approximation and density gradient approximation models, it can be written as

$$n^Q = const. \times (x - x_{interface})^2. \tag{3.8}$$

Therefore, some assumptions are exhibited as follows. The sheet charge density N_s in the boundary has the form of

$$N_s = \int_0^{\frac{1}{2}dx_1} (p(x) - n(x) + N_D^+(x) - N_A^-(x))dx, \tag{3.9}$$

where $dx_1 = x_1 - x_0$, which means the difference between first and second mesh in numerical simulation and $N_D^+(x) - N_A^-(x) \approx -N_A(x)$. $p(x)$ and $N_A(x)$ are the hole density and substrate doping concentration, respectively, which can be treated as constants equal to p_0 and N_{A0} in the dx_1. If $dx_1 \ll \lambda_{th}$, Eq. 3.9 becomes

$$N_s = (p_0 - N_{A0})\frac{1}{2}dx_1 + \int_0^{\frac{1}{2}dx_1} n(x)dx. \tag{3.10}$$

The potential within dx_1 is regarded as constant because dx_1 is very small. By these approximations, n^Q in the boundary is proportional to x^2, given by

$$n^Q_{bounary} = N_C \exp(-\frac{q\phi_F - q\psi}{k_B T}) \cdot (\frac{x^2}{\lambda^2_{th}}). \tag{3.11}$$

And Eq. (3.7) can be modified by Fermi-Dirac statics, shown as

$$n^Q(x) = N_C F_{1/2}(-\frac{q\phi_F - q\psi(x)}{k_B T})[1 - \exp(-\frac{x^2}{\lambda^2_{th}})]. \tag{3.12}$$

The H$\ddot{a}$nsch's model has more physical meanings than Van Dort's model described above, but it has the shortcoming that the adjustable mathematical parameter m_k is very sensitive by different cases, for example, different substrate doping, gate oxide thickness and applied gate voltage may all need exclusive m_k to have accurate enough results compared with the Schr$\ddot{o}$dinger-Poisson self-consistent ones. It is not so convenient for real applications but may be treated as the initial guesses for other quantum correction models which are discussed as follows.

3.3 The Li's Model

This model [21] improves H$\ddot{a}$nsch's model to have a more accurate electron distribution and the peak value of electron. It has a very close results compared with Schr$\ddot{o}$dinfer-Poisson's. However, the difficulty is how to extract three parameters shown below. In the paper [21], they are extracted by the optimization theory. The model is shown as

$$n_Q(x) = a_0 n_{CL}(x) \cdot (1 - exp[-a_1 \xi^2 (1 - \frac{1}{2}(\frac{\xi}{\xi_0})^2) - a_2 \xi^3]), \tag{3.13}$$

where $n_{CL}(x)$ is the classical electron density solved with the Poisson equation, $\xi = x/\lambda_{th}$ and λ_{th} is the thermal wavelength. For the double-gate case, $\xi_0 = T_{si}/2\lambda_{th}$, where T_{si} is the thickness of silicon body. a_0, a_1 and a_2 are optimized and calibrated with the Schrödinger-Poisson solutions by optimization theory.

3.4 The Modified Local Density Approximation Model

Paasch and Ubensee firstly proposed a quantum correction model called modified local density approximation model which is applicable even if there is a abrupt variance in potential [17]. In the case of interface of Si/SiO$_2$, the quantum corrected electron density is approximated by adding an additional correction term into the classical model in an integration form, given by

$$\begin{aligned} n^Q(x) &= N_C \frac{2}{\sqrt{\pi}} \int_0^\infty \frac{d\xi \cdot \xi^{0.5}}{1 + \exp(\xi - k(x))} \\ &- N_C \frac{2}{\sqrt{\pi}} \int_0^\infty \frac{d\xi \cdot \xi^{0.5}}{1 + \exp(\xi - k(x))} \Sigma_{i=1}^6 j_0 \frac{(2x\sqrt{\xi}/\lambda_n^i)}{6} \\ &= N_C \frac{2}{\sqrt{\pi}} \int_0^\infty \frac{d\xi \cdot \xi^{0.5}}{1 + \exp(\xi - k(x))} [1 - \Sigma_{i=1}^6 j_0 \frac{(2x\sqrt{\xi}/\lambda_n^i)}{6}], \end{aligned} \tag{3.14}$$

where,

$$\begin{aligned} \xi &= \frac{E - E_c)}{k_B T}, \\ k(x) &= \frac{E_F + q\psi(x)}{k_B T}, \quad \texttt{and} \\ \lambda_n^i &= \sqrt{\frac{\hbar^2}{2m_n^{i*} k_B T}}. \end{aligned} \tag{3.15}$$

x is the distance counted from the interface, N_C is conduction band effective density-of-state, j_0 is the zeroth-order spherical Bessel function, E_F is fermi level, and λ_{th} is the thermal wavelength as described above.

The effective mass is usually considered to take an average value between longitudinal and transverse ones because the six-fold ellipse-shape symmetry of valleys when calculating the spherical Bessel function j_0. Note that the model smooths the curve behavior between quantum and classical regimes. For region which is far from the Si/SiO$_2$ interface, Eq. (3.14) becomes

$$n(x) = N_C \frac{2}{\sqrt{\pi}} \int_0^\infty \frac{d\xi \cdot \xi^{0.5}}{1 + \exp(\xi - k(x))}. \tag{3.16}$$

At $x = 0$, Eq. (3.16) gives $n(x) = 0$, which is consistent with the assumption that wave function vanishes at the boundary. The thermal wavelength λ_{th} is a characteristic length which depends on the temperature and the effective mass m_n^* can been seem to be a adjustable parameter to fit Schrödinger-Poisson solutions. MLDA model is much more efficient to solve a numerical integration than a Schrödinger-Poisson solver which need to solve an eignevalue problem. Besides, the fitting parameter m_k is less sensitive than

H$\ddot{a}$nsch model. It is the advantage when implanted into the device simulators.

3.5 The Ferry's Effective Potential Model

In analogy to the smoothed potential representations for the quantum hydrodynamic model (density-gradient model), David K. Ferry suggested an effective potential model that emerges from the wave packet description of particle motion, where the extent of the wave packet spread is obtained from the range of wave vectors in the thermal distribution function [18][19]. This form for the effective potential allows one to build in certain quantum effects that arise from the non-zero size of the electron wave packet. It can be derived from potential part of the Hamiltonian, given by

$$H_v = \int drV(r)n(r). \tag{3.17}$$

Using the wavepacket description leads to

$$\begin{aligned} H_v &= \int drV(r)\sum_i n_i(r) \\ &= \int drV(r)\sum_i \int dr'exp(-\frac{|r-r'|^2}{a^2})\delta(r'-r_i) \\ &= \sum_i \int dr\delta(r'-r_i)\int dr'V(r')exp(-\frac{|r-r'|^2}{a^2}). \end{aligned} \tag{3.18}$$

The primed integration is defined as effective potential, V^Q, and the finite size of the electron size is replaced by smoothing the Hatree potential with a Gaussian integration shown as

$$V^Q(x) = \int V(x+\xi)G(\xi, a_0)d\xi, \tag{3.19}$$

where G is a Gaussian with the standard deviation a_0. a_0 is defined as $a_0 = \hbar/\sqrt{8m^* k_B T}$. In three dimensions, it becomes

$$\begin{aligned} V^Q(x,y,z) &= \frac{1}{(2\pi)^{1.5}a_x a_y a_z}\int\int\int V(x',y',z') \\ &\quad \exp(-\frac{(x-x')^2}{2a_x^2} - \frac{(y-y')^2}{2a_y^2} - \frac{(z-z')^2}{2a_z^2})dx'dy'dz', \end{aligned} \tag{3.20}$$

where $V(x',y',z')$ is the classical potential and $a_{x,y,z}$ are the standard deviations of Gaussian integration. This model is easy to integrate into the classical models. The effective potential V^Q is related to the self-consistent potential obtained from Poisson equation. We just need to perform an integral-smoothing transformation to original potential with gaussian function. We can expand Eq. (3.19) in Taylor series. The one-dimensional case becomes

$$\begin{aligned} V^Q(x) &= \frac{1}{\sqrt{2\pi}a_0}\int_{-\infty}^{\infty} V(x+\xi)exp(-\frac{\xi^2}{2a_0^2})d\xi \\ &\cong \frac{1}{\sqrt{2\pi}a_0}\int_{-\infty}^{\infty}[V(x) + \xi\frac{\partial V}{\partial x} + \frac{\xi^2}{2}\frac{\partial^2 V}{\partial x^2} + \cdots]exp(-\frac{\xi^2}{2a_0^2})d\xi. \\ &= V(x) + a_0^2\frac{\partial^2 V}{\partial x^2} + \cdots . \end{aligned} \tag{3.21}$$

In nondegenerate semiconductors, V can be described by $(ln\frac{n}{n_0})/(-\beta)$, Eq. (3.21) becomes

$$\begin{aligned} V^Q(x) &= V(x) - \frac{2a_0^2}{\beta}\frac{\partial^2 ln(\sqrt{n/n_0})}{\partial x^2} + \cdots \\ &= V(x) - \frac{2a_0^2}{\beta\sqrt{n}}\frac{\partial^2\sqrt{n}}{\partial x^2} + \cdots . \end{aligned} \tag{3.22}$$

Therefore, Ferry's effective potential is related to the relation of gradient of density term, which is usually known as Bohm potential. Although the effective potential model has the advantage that it is a convenient way to produce a first-order result, drawbacks such as solution is overestimated and peak location is further setback from the material interfaces are inevitable.

Chapter 4

Implicit Quantum Corrections

In the chapter, the implicit quantum corrections, i.e. The density-gradient model, effective conduction band edge model and thermodynamic approximation model, are discussed in terms of theoretical viewpoint.

4.1 The Density-Gradient Model

The quantum potential originates from hydrodynamic formulation of quantum mechanics by Bohm and is developed by Ancona is called density-gradient model [13]-[15]. Begin from the one-particle Schrödinger equation, of the form

$$i\hbar\frac{\partial\psi}{\partial t} = -\frac{\hbar^2}{2m}\nabla^2\psi + V(x)\psi. \tag{4.1}$$

The wave function is written in complex form in terms of its amplitude $R(r,t)$ and phase $S(r,t)$ as

$$\psi(r,t) = R(r,t)\exp(\frac{iS(r,t)}{\hbar}). \tag{4.2}$$

Then substituted back into the Schr$\ddot{o}$dinger equation, one arrives at the following coupled equations for the density and phase given as

$$\frac{\partial R(r,t)}{\partial t} = -\frac{1}{2m}[R(r,t)\nabla^2 S(r,t) + 2\nabla R(r,t)\cdot\nabla S(r,t)], \tag{4.3}$$

and

$$\frac{\partial S(r,t)}{\partial t} = -[\frac{[\nabla S(r,t)]^2}{2m} + V(r,t) - \frac{\hbar^2}{2m}\frac{\nabla^2 R(r,t)}{R(r,t)}]. \tag{4.4}$$

We can write $\rho(r,t) = R(r,t)^2$, where $\rho(r,t)$ is the probability density and obtain

$$\frac{\partial \rho(r,t)}{\partial t} + \nabla\cdot[\rho(r,t)\frac{1}{m}\nabla S(r,t)] = 0, \tag{4.5}$$

and

$$-\frac{\partial S(r,t)}{\partial t} = \frac{[\nabla S(r,t)]^2}{2m} + V(r,t) + V^Q. \tag{4.6}$$

In the classical limit, the above equation are subject to a very simple interpretation. The function $S(r,t)$ is a solution of the Hamiltonian-Jacobi equation. If we consider an ensemble of particle trajectories which are solutions of the equations of motion, if all these trajectories are normal to any given surface of constant S, then they are normal to all sureface of constant S. And $\frac{\nabla S(r,t)}{m}$ means the velocity vector. Eq. 4.5 can be written as

$$\frac{\partial \rho(r,t)}{\partial t} + \nabla\cdot[\rho(r,t)v] = 0. \tag{4.7}$$

Since $\rho(r,t)$ is the probability density, ρv isthe mean current of particles in this ensemble, and Eq. (4.7) expresses continuity equation. Eq. (4.5) and Eq. (4.6) have the form of classical hydrodynamic equations with a additional potential, often referred to as the quantum potential (Bohm potential) [44], shown as

$$V^Q = -\frac{\hbar^2}{2mR}\nabla^2 R = -\frac{\hbar^2}{2m\sqrt{n}}\frac{\partial^2\sqrt{n}}{\partial x^2}, \tag{4.8}$$

where the density n is related to the probability density as $n(r,t) = N\rho(r,t) = NR(r,t)^2$, N is the total number of particles in the ensemble. Nevertheless, an extra term is introduced in the carrier flux by making the equation of state for the electron desity-gradient dependance. The current density is corrected as

$$\overrightarrow{J_n} = -qn\mu_n\nabla\psi + qD_n\nabla n - qn\mu_n\nabla(2b_n\frac{\nabla^2\sqrt{n}}{\sqrt{n}}), \tag{4.9}$$

where b_n is the density-gradient coefficient which determines the strength of the gradient effect in the electron gas. The last term in the right hand side of Eq. (4.9) is referred to as ”quantum diffusion”, which makes the electron continuity equation has a fourth-order partial differential equation. Therefore, such an approach is highly sensitive to noise in the local carrier density, and the methodology is highly important in cases of strong quantization. However, advantages of not so sensitive parameter b_n compared with other quantum approximation models and results close to Schr$\ddot{o}$dinger-Poisson solutions make the density-gradient model is commonly used in commercial semiconductor simulators for quantum correction.

The density-gradient equation may be simplified to a simpler form, say modified density-gradient equation. We note that a similar idea has been proposed [20]. Eq. (4.8) can be represented by

$$\begin{aligned} V^{*}(r) &= V^{cl}(r) - V^{Q}(r), \\ &= V^{cl}(r) - \frac{\hbar^2}{2mr}\frac{\nabla^2\sqrt{n}}{\sqrt{n}}, \\ &= V^{cl}(r) - \frac{\hbar^2}{4mr}[\nabla^2 lnn(r) + \frac{1}{2}(\nabla lnn(r))^2], \end{aligned} \tag{4.10}$$

where V^{*} is the effective total potential energy and V^{cl} is the classical potential. r is chosen between 1 and 3. For obtaining the effective conduction-band edge equation, we propose that in the equilibrium Boltzmann distribution, after quantum correction, $lnn(r)$ is proportional to $-V^{*}(r)/k_BT$ and not to $-V(r)/k_BT$. Thus, Eq. (4.10) becomes

$$V^{*}(r) = V^{cl}(r) + \frac{\hbar^2}{4mrk_BT}[\nabla^2 V^{*}(r) - \frac{1}{2k_BT}(\nabla V^{*}(r))^2]. \tag{4.11}$$

The effective conduction-band edge equation has the improvement that no serious request for a very well defined mesh, as used in general density-gradient equation because the high-order differential of carrier density is replaced by effective total potential energy.

4.2 Thermodynamic Approached Effective Potential Model

There is an alternative to the approach outlined above. The mean idea of a thermodynamic approached effective potential model is essentially a perturbation theory around thermal equilibrium [22][45]. We seek a semiclassical transport equation with a quantum corrected potential whose classical commutator, $[\varepsilon^{eff}, f]_{classical}$ will produce the same thermal equilibrium state as Wigner commutator $[\varepsilon, f]_W$, where f is a distribution function evaluated from Weyl quantization [46]. The process is detailed in the next sections.

4.2.1 Classical and Quantum Collisionless Boltzmann Equations

We start from transforming the many-body Schr$\ddot{o}$dinger-Poisson system to a analog of the collisionless Boltzmann-Poisson equations which assumes mean field theories and effective mass approximations for ensemble by use of Wigner transformation, given by [46][47]

$$f(x,p,t) = (2\pi)^{-3}\int_{R^3} \rho(x+\frac{\hbar}{2}\eta, x-\frac{\hbar}{2}\eta) exp(i\eta \cdot p) d\eta, \tag{4.12}$$

where

$$\rho(x,y,t) = \Sigma_\lambda F(\lambda)\psi_\lambda(x)^*\psi_\lambda(y). \tag{4.13}$$

$\rho(x,y,t)$ means the density matrix of mixed state and ψ_λ is wave function with eigen energy λ. The Wigner function satisfies the Wigner, or collisionless quantum Boltzmann equation

$$\begin{aligned} &\partial_t f + [\varepsilon, f]_W = 0, \quad \varepsilon = \frac{|p|^2}{2m^*} + eV(x,t) \\ \Rightarrow \quad &\partial_t f + \frac{i}{\hbar}\sum_{\upsilon=\pm 1} \upsilon\varepsilon(x + \frac{i\upsilon\hbar}{2}\nabla_p, p - \frac{i\upsilon\hbar}{2}\nabla_x) f = 0 \end{aligned}$$

and

$$\Rightarrow \quad \partial_t f + \frac{1}{m^*}\nabla_x \cdot (pf) - \frac{ie}{\hbar}[V(x + \frac{\hbar}{2i}\nabla_p) - V(x - \frac{\hbar}{2i}\nabla_p)] = 0, \tag{4.14}$$

which can be taken as a pseudodifferentail operators $\theta[V]$ by

$$\partial_t f + \frac{1}{m^*}\nabla_x \cdot (pf) - e\theta[V] f = 0, \tag{4.15}$$

where

$$\theta[V] = \frac{i}{\hbar}[V(x + \frac{\hbar}{2i}\nabla_p) - V(x - \frac{\hbar}{2i}\nabla_p)]. \tag{4.16}$$

And the action of $\theta[V]$ is given by

$$\begin{aligned} \theta[V] f(x,p,t) \quad &= \quad (2\pi)^{-3}\int_{R^3}\int_{R^3} \frac{i}{\hbar}[V(x + \frac{\hbar}{2}\eta) - V(x - \frac{\hbar}{2}\eta)] \\ &\cdot \quad f(x,q,t) exp[i\eta \cdot (p-q)] dq d\eta. \end{aligned} \tag{4.17}$$

In the effective potential approach, one replaces the quantum Boltzmann equation by a corresponding semiclassical equation with a modified potential. Thus, Wigner commutator

$[\varepsilon, f]_W$ is replaced by the classical commutator $[\varepsilon^{eff}, f]_{classical}$, the semiclassical Boltzmann equation is given by

$$\begin{aligned} &\partial_t f + [\varepsilon^{eff}, f]_{classical} = 0, \quad \varepsilon = \frac{|p|^2}{2m^*} + eV^{eff}(x,t), \\ \Rightarrow \quad &\partial_t f + \nabla_p \varepsilon^{eff} \cdot \nabla_x f - \nabla_x \varepsilon^{eff} \cdot \nabla_p f = 0, \end{aligned}$$

and

$$\Rightarrow \quad \partial_t f + \frac{1}{m^*} \nabla_x \cdot (pf) - e\nabla_p \cdot (\nabla_x V^{eff} f) = 0. \tag{4.18}$$

Therefore, all quantum effects are taken into account by the force acting on the electron. The quantum corrections through the semiclassical transport equations are Wigner-Boltzmann-Poisson system shown below,

$$\begin{aligned} &\partial_t f + \frac{1}{m^*} \nabla_x \cdot (pf) - e\theta[V]f = Q(f), \\ &\nabla \cdot \varepsilon \nabla V = e(n - D), \\ &n(x,t) = \int_{R^3} f(x,p,t)dp, \end{aligned} \tag{4.19}$$

where $Q(f)$ denotes the collision operator when considering collision process and it's zero when modelling collisionless one. e denotes the electron charge, D is the doping concentration and $n(x,t)$ means the density of electrons.

4.2.2 Approximations to Thermal Equilibrium

The effective potential is based on the perturbation theory around thermal equilibrium. We want to find a semiclassical transport equation with a quantum corrected potential whose classical commutator, $[\varepsilon^{eff}, f]_{classical}$ will produce the same thermal equilibrium state as Wigner commutator $[\varepsilon, f]_W$ when applying to a quantum system. Our purpose is to make the two operators shown above equal to each other and then extract the effective potential to be used in semiclassical transport equations [22].

First, starting from the Wigner-Boltzmann-Poisson system, Eq. (4.19) and transform it to center-of-mass coordinates. The mean velocity u(x,t) of the ensemble is defined as

$$\int_{R^3} pf(x,p,t)dp = m^* un(x,t), \quad n(x,t) = \int_{R^3} f(x,p,t)dp, \tag{4.20}$$

and then choose m^*u to be the origin of the center-of-mass coordinates in momentum space. Make the Lagrangian transformation to Wigner equation, shown as [22]

$$\partial_t f^L + \frac{1}{m^*}\nabla_x \cdot [(p+m^*u)f^L] - \nabla_p \cdot f^L[m^*\partial_t u + ((p+m^*u)\cdot\nabla_x)u] - e\theta[V]f^L = Q^L(f^L), \tag{4.21}$$

where $f^L(x,p,t) = f(x, p+m^*u(x,t), t)$ and $Q^L(f^L)(x,p,t) = Q(f)(x, p+m^*u, t)$.

The thermal equilibrium in classical case have the form of

$$\begin{aligned} & f^{eq} = \hbar^{-3} exp(-\beta\varepsilon^{eff}), \\ \Rightarrow \quad & f^L(x,p,t) \approx f^{eq}(x,p,t) = exp[-\frac{\beta|p|^2}{2m^*} - \beta e V^Q(x,p,\beta)]. \end{aligned} \tag{4.22}$$

On the other hand, in the quantum mechanics, the thermal equilibrium state is defined as a density matrix as [48][49]

$$\rho^{eq} = exp(-\beta H), \tag{4.23}$$

where H is the Hamiltonian operator and β is $1/k_B T$. Taking use of the definition of Wigner function, i.e. Weyl quantization,

$$\begin{aligned} & f^{eq}(x,p,t) = (2\pi)^{-3} \int_{R^3} \rho^{eq}(x + \frac{\hbar}{2}\eta, x - \frac{\hbar}{2}\eta) exp(i\eta \cdot p) d\eta, \\ & \rho^{eq}(x,y) = \sum_{\lambda} exp[\beta(\phi - \lambda)] \psi_{\lambda}^{eq}(x)^{*} \psi_{\lambda}^{eq}(y), \\ & (-\frac{\hbar^2}{2m^*}\Delta + eV)\psi_{\lambda}^{eq} = \lambda \psi_{\lambda}^{eq}. \end{aligned} \tag{4.24}$$

Therefore, the effective potential can be derived approximately from substituting $exp(-\beta\varepsilon^{eff})$ for Weyl quantization of $exp(-\beta H)$ [50]. Now we already have a description for classical case in thermal equilibrium, and then the next step is to get an analytical solution of quantum state of thermal equilibrium. The procedure is shown in the following section.

4.2.3 Thermodynamic Effective Potential

We need to find a explicit expression in quantum distribution function in thermal equilibrium, f^{eq}, in order to get a formula of effective potential V^{eff}. Of course, it is not possible to obtain a analytical expression of V^{eff}, so the approximations are introduced

[48][49][51]. The Bloch equation is a formal way to replace the computation of the exponential of a density matrix by the solution of a parabolic differential equation.

In Eq. (4.24), we have the expression of density matrix by thermal equilibrium state is defined as a density matrix as

$$\rho^{eq}(x,y) = \sum_{\lambda} exp[\beta(\phi-\lambda)]\psi_{\lambda}^{eq}(x)^{*}\psi_{\lambda}^{eq}(y), \tag{4.25}$$

then differentiate ρ^{eq} with respect to β, which gives

$$\partial_{\beta}\rho^{eq}(x,y,\beta) = \sum_{\lambda} exp[\beta(\phi-\lambda)](\phi-\lambda)\psi_{\lambda}^{eq}(x)^{*}\psi_{\lambda}^{eq}(y), \tag{4.26}$$

and make the Hamiltonian H to density matrix ρ^{eq} gives

$$H\rho^{eq} = \sum_{\lambda} exp[\beta(\phi-\lambda)]\lambda\psi_{\lambda}^{eq}(x)^{*}\psi_{\lambda}^{eq}(y) = \rho^{eq}H. \tag{4.27}$$

Rearrange Eq. (4.26) and Eq. (4.27), the equilibrium density matrix ρ^{eq} satisfies an initial value problem

$$\partial_{\beta}\rho^{eq}(x,y,\beta) = -\frac{1}{2}(H\rho^{eq}+\rho^{eq}H)+\phi\rho^{eq}, \rho^{eq}(x,y,0) = \delta(x-y), \tag{4.28}$$

or

$$\partial_{\beta}\rho^{eq}(x,y,\beta) = \frac{\hbar^2}{4m^*}(\Delta_x+\Delta_y)\rho^{eq} - \frac{e}{2}[V(x)+V(y)]\rho^{eq}+\phi\rho^{eq}, \quad \rho^{eq}(x,y,0) = \delta(x-y). \tag{4.29}$$

Eq. (4.29) is called the Bloch equation for density matrix ρ^{eq} which is symmetrized to be real and self adjoint. The next step, use the Weyl quantization, Eq. (4.24), to get the expression of f^{eq} from ρ^{eq}. An initial value problem is given by

$$\partial_\beta f^{eq}(x,y,\beta) = \frac{\hbar^2}{8m^*}\Delta_x f^{eq} - \frac{|p|^2}{2m^*} f^{eq} - e\omega[V]f^{eq} + \phi f^{eq}, \quad f^{eq}(x,y,0) = \hbar^{-3}, \tag{4.30}$$

with the pseudodifferential operator ω given by

$$\omega[V] = \frac{1}{2}[V(x + \frac{\hbar}{2i}\nabla_p) + V(x - \frac{\hbar}{2i}\nabla_p)], \tag{4.31}$$

and the action of $\omega[V]$ is given by

$$\omega[V]f(x,p) = \frac{1}{2}(2\pi)^{-3}\int_{R^3}\int_{R^3}[V(x+\frac{\hbar}{2}\eta) + V(x-\frac{\hbar}{2}\eta)]f(x,q)exp[i\eta\cdot(p-q)]dqd\eta. \tag{4.32}$$

Eq. (4.30) is solved by Borm approximation [48][49] which assume that the Laplacian in Eq. (4.30) dominates the potential term. We set $V = \varepsilon V_\varepsilon$, expanding the solution of Eq. (4.30) in powers of ε and setting $f^{eq} = \hbar^{-3}(f_0 + \varepsilon f_1 + \ldots) \approx (f_0 + \varepsilon f_1)$, where ε is a formal parameter. Therefore, Eq. (4.30) becomes [22]

$$\begin{aligned} &\partial_\beta f^{eq}(x,y,\beta) = \alpha\Delta_x f^{eq} - \frac{|p|^2}{2m^*} f^{eq} - e\varepsilon\omega[V_\varepsilon]f^{eq} + \phi f^{eq}, \quad f^{eq}(x,y,0) = \hbar^{-3}, \\ \Rightarrow\ &\partial_\beta \hbar^{-3} f_0 + \hbar^{-3}\varepsilon\partial_\beta f_1 = \alpha\hbar^{-3}\Delta_x f_0 + \alpha\hbar^{-3}\Delta_x f_1 - \frac{|p|^2}{2m^*}\hbar^{-3} f_0 - \frac{|p|^2}{2m^*}\hbar^{-3}\varepsilon f_1 \\ &-e\varepsilon\hbar^{-3} f_0\omega[V_\varepsilon] - e\varepsilon^2\hbar^{-3} f_1\omega[V_\varepsilon] + \phi\hbar^{-3} f_0 + \phi\hbar^{-3}\varepsilon f_1, \end{aligned} \tag{4.33}$$

where α denotes $\hbar^2/8m^*$. Eq. 4.33 can be divided into two terms of [22]

$$\partial_\beta f_0(x,y,\beta) = \alpha\Delta_x f_0 - \frac{|p|^2}{2m^*} f_0 + \phi f_0, f_0(x,p,0) = 1, \tag{4.34}$$

and

$$\partial_\beta f_1(x,y,\beta) = \alpha \Delta_x f_1 - \frac{|p|^2}{2m^*} f_1 - e\varepsilon[V_\varepsilon] f_0 + \phi f_1, f_1(x,p,0) = 0. \tag{4.35}$$

Eq. (4.34) can be solved easily and obtain

$$f_0 = exp[\beta\phi - \frac{\beta|p|^2}{2m^*}]. \tag{4.36}$$

We deal with Eq. (4.35) by Fourier transforming in space and make f_1 acted by a pseudodifferential operator on V_ε. Define [22]

$$\begin{aligned} g(\xi,p,x) &= (2\pi)^{-3} \int_{R^3} f_1(x,p,\beta) exp(-i\xi\cdot x)dx, \\ \hat{V}(\xi) &= (2\pi)^{-3} \int_{R^{-3}} V_\varepsilon(x) exp(-i\xi\cdot x)dx, \end{aligned} \tag{4.37}$$

and obtain

$$\partial_\beta g(\xi,p,\beta) = -\alpha|\xi|^2 g - \frac{|p|^2}{2m^*} g - eR(\xi,p,\beta)\hat{V} + \phi g, g(\xi,p,0) = 0, \tag{4.38}$$

where

$$R(\xi,p,\beta)\hat{V}(\xi) = (2\pi)^{-3} \int_{R^3} \omega[V_\varepsilon] f_0(x,p,\beta) exp(-i\xi\cdot x)dx, \tag{4.39}$$

Use the definition of pseudodifferential operator $\omega[V_\varepsilon]$ to obtain

$$R(\xi,p,\beta)\hat{V}(\xi) = (2\pi)^{-3}\frac{1}{2}(2\pi)^{-3}\int_{R^3}\int_{R^3}\int_{R^3}[V_\varepsilon(x+\frac{\hbar}{2}\eta)+V_\varepsilon(x-\frac{\hbar}{2}\eta)]f_0$$

$$\cdot exp[-i\xi+\eta(p-q)]dqd\eta dx,$$

$$\Rightarrow \quad R(\xi,p,\beta) = \frac{1}{2}(2\pi)^{-\frac{3}{2}}exp(\beta\phi)\int_{R^3}exp[i\sqrt{\frac{\beta}{m^*}}\eta\cdot(p+\frac{\hbar}{2}\xi)-\frac{|\eta|^2}{2}]$$

$$+exp[i\sqrt{\frac{\beta}{m^*}}\eta\cdot(p-\frac{\hbar}{2}\xi)-\frac{|\eta|^2}{2}]d\eta,$$

$$\Rightarrow \quad R(\xi,p,\beta) = \frac{1}{2}exp(\beta\phi)[exp(-\frac{\beta}{2m^*}|p+\frac{\hbar}{2}\xi|^2)+exp(-\frac{\beta}{2m^*}|p-\frac{\hbar}{2}\xi|^2)]. \quad (4.40)$$

Eq. (4.40) is substituted into Eq. (4.38) to yield

$$\begin{aligned}\partial_\beta g(\xi,p,\beta) &= -\alpha|\xi|^2 g - \frac{|p|^2}{2m^*}g - e(\frac{1}{2}exp(\beta\phi)[exp(-\frac{\beta}{2m^*}|p+\frac{\hbar}{2}\xi|^2)\\ &\quad +exp(-\frac{\beta}{2m^*}|p-\frac{\hbar}{2}\xi|^2)])\hat{V}+\phi g, g(\xi,p,0)=0,\end{aligned} \quad (4.41)$$

The ordinary differential equation is solved to give

$$g(\xi,p,\beta) = -e\beta\hat{V}(\xi)exp(-\alpha\beta|p|^2-\frac{\beta|p|^2}{2m^*}+\beta\phi)\int_0^1 cosh(\frac{\gamma\beta\hbar}{2m^*}p\cdot\xi)d\gamma. \quad (4.42)$$

Reversing the Fourier transforms, we obtain f_1 as

$$\begin{aligned}f_1(x,p,\beta) = -e\beta(2\pi)^{-3}\int_{R^3}\int_{R^3}\int_0^1 V_\varepsilon(y)exp(-\alpha\beta|\xi|^2-\frac{\beta|p|^2}{2m^*}+\beta\phi)\\ \cdot cosh(\frac{\gamma\beta\hbar}{2m^*}p\cdot\xi)exp[i\xi\cdot(x-y)]d\gamma dyd\xi.\end{aligned} \quad (4.43)$$

f_1 can be expressed by a pseudodifferential operator S acting on V_ε, shown as

$$f_1(x,p,\beta) = -exp(\beta\phi)S(-i\nabla_x,p,\beta)V_\varepsilon, \quad (4.44)$$

where S is given by

$$\begin{aligned} S(\xi,p,\beta) &= \frac{e\beta}{2}\int_0^1 exp[\alpha\beta(\gamma^2-1)|\xi|^2-\frac{\beta}{2m^*}|p+\frac{\gamma\hbar}{2}\xi|^2] \\ &+ exp[\alpha\beta(\gamma^2-1)|\xi|^2-\frac{\beta}{2m^*}|p-\frac{\gamma\hbar}{2}\xi|^2]d\gamma. \end{aligned} \tag{4.45}$$

Combining Eq. (4.36) and Eq. (4.44) regarding $f^{eq}=\hbar^{-3}(f_0+\varepsilon f_1)$ and $V=\varepsilon V_\varepsilon$, we obtain

$$\begin{aligned} &\hbar^{-3}f^{eq}(x,p,\beta)\approx f_0+\varepsilon f_1, \\ \Rightarrow\ &\hbar^{-3}f^{eq}(x,p,\beta)\approx exp(\beta\phi-\frac{\beta|p|^2}{2m^*})-\varepsilon exp(\beta\phi)S(-i\nabla_x,p,\beta)V_\varepsilon, \\ \Rightarrow\ &\hbar^{-3}f^{eq}(x,p,\beta)\approx exp(\beta\phi)[exp-(\frac{\beta|p|^2}{2m^*})-\varepsilon S(-i\nabla_x,p,\beta)V_\varepsilon], \\ \Rightarrow\ &\hbar^{-3}f^{eq}(x,p,\beta)\approx exp(\beta\phi)[exp-(\frac{\beta|p|^2}{2m^*})-S(-i\nabla_x,p,\beta)V]. \end{aligned} \tag{4.46}$$

Now the approximative formula, Eq. (4.46), for quantum state of thermal equilibrium is derived. We just only need to let the semiclassical state in thermal equilibrium equal to the quantum one, then the form of effective potential is extracted, which is shown as

$$\begin{aligned} \hbar^{-3}f^{eq}(x,p,\beta) &= exp(\beta\phi)[exp-(\frac{\beta|p|^2}{2m^*})-S(-i\nabla_x,p,\beta)V(x)] \\ &= exp[\beta\phi-\frac{\beta|p|^2}{2m^*}-\beta eV^{eff}(x,p,\beta)]. \\ \Rightarrow V^{eff}(x,p,\beta) &= \frac{1}{e\beta}exp(\frac{\beta|p|^2}{2m^*})S(-i\nabla_x,p,\beta)V(x), \end{aligned} \tag{4.47}$$

where S is defined as Eq. (4.45) and can be simplified to give

$$S(\xi,p,\beta)=e\beta exp-(\frac{\beta|p|^2}{2m^*}-\alpha\beta|\xi|^2)\int_0^1 cosh(\frac{i\beta\hbar p\cdot\xi}{2m^*})d\gamma. \tag{4.48}$$

Combining Eq. (4.47) and Eq. (4.48), V^{eff} is given by

$$V^{eff}(x,p,\beta) = exp(\alpha\beta|\nabla_x|^2)\frac{2m^*}{i\beta\hbar p\cdot\nabla_x}sinh(\frac{i\beta\hbar p\cdot\nabla_x}{2m^*})V(x), \tag{4.49}$$

or

$$V^{eff}(\xi,p,\beta) = (2\pi)^{-3}\int_{R^3}\int_{R^3} exp(-\frac{\beta\hbar^2|\xi|^2}{8m^*})\frac{2m^*}{\beta\hbar p\cdot\xi}sinh(\frac{\beta\hbar p\cdot\xi}{2m^*})V(y)exp[i\xi\cdot(x-y)]dyd\xi, \tag{4.50}$$

with a pseudodifferential operator expression. Note that if we approximate $sinh(\frac{\beta\hbar p\cdot\xi}{2m^*})$ to $\frac{\beta\hbar p\cdot\xi}{2m^*}$, the classical potential is smoothed by a Gaussian-type integral. Therefore, the thermodynamic effective potential has the smoothing effect of potential just like what Ferry's effective potential does.

We summarize the derivation procedure of thermodynamic approach described above in Fig. 4.1. We start from the Wigner equation-Poisson system, then note that the pseudodifferential operator $\theta[V]$ has different appearances in the case of classical and quantum cases. We seek a semiclassical transport equation with a quantum corrected potential whose classical commutator, $[\varepsilon^{eff}, f]_{classical}$ will produce the same thermal equilibrium state as Wigner commutator $[\varepsilon, f]_W$, so we want to find an analytical form of quantum and classical distribution function in order to derive an explicit quantum potential by transposition. First, we transfer Wigner equation to center-of-mass coordinates and then introduce the thermal equilibrium expression. By Born approximation, distribution function of Wigner equation is simplified to an explicit form. Make the distribution function of quantum and classical cases equal to each. Finally, the thermodynamic effective potential is extracted.

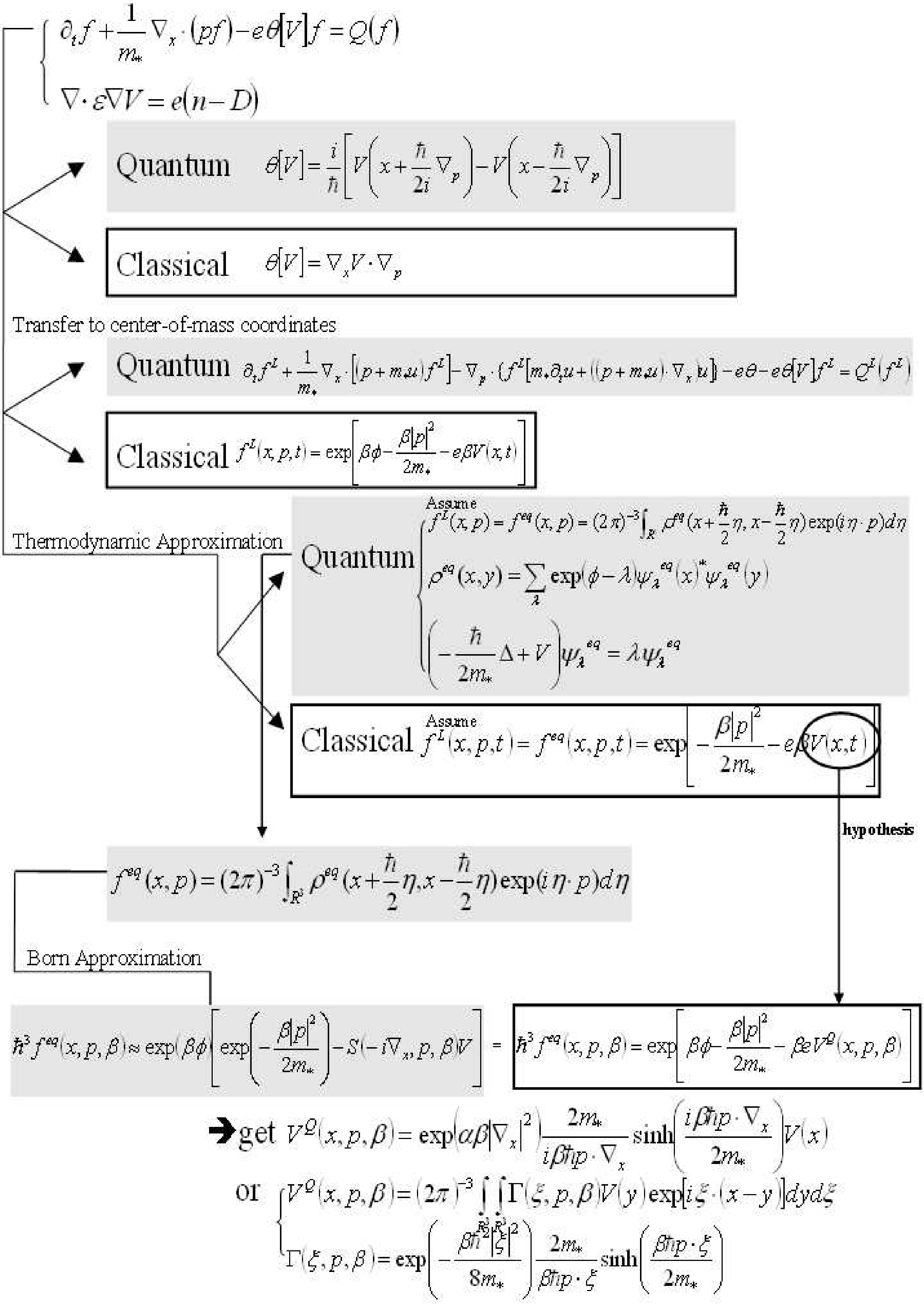

Figure 4.1: The flow chart of thermodynamic approach.

4.2.4 Quantum Barrier Field

Eq. (4.49) shows the expression of the thermodynamic effective potential successfully. V^{eff} and V in Eq. (4.49) can be divided into two terms [51], $V_B^{eff} + V_H^{eff}$ and $V_B + V_H$, respectively. given by

$$V_B^{eff}(x,p,\beta) = exp(\alpha\beta|\nabla_x|^2)\frac{2m^*}{i\beta\hbar p\cdot\nabla_x}sinh(\frac{i\beta\hbar p\cdot\nabla_x}{2m^*})V_B(x), \tag{4.51}$$

and

$$V_H^{eff}(x,p,\beta) = exp(\alpha\beta|\nabla_x|^2)\frac{2m^*}{i\beta\hbar p\cdot\nabla_x}sinh(\frac{i\beta\hbar p\cdot\nabla_x}{2m^*})V_H(x). \tag{4.52}$$

V_B models the discontinuous barrier accounting for the interface between silicon and silicon dioxide in a MOSFET. Not that V_B is only one-dimensional along the direction orthogonal to the interface. And the V_H is evaluated from Poisson's equation, which is two-dimensional and time dependant. But since in many applications the quantum action of the Coulomb potential is negligible [51][52], or, only the concentration of the channel doping is higher than 5e18, i.e. heavily channel doping, the quantum effect accounting for Coulomb potential will make the potential curve various greater than 4 percent comparing with the classical potential. Thus, quantum effect of Coulomb potential computed from Poisson's equation can be neglected when channel is lightly doped. Adopting the classical Coulomb potential for analysis of advanced device is sufficient because channels of devices nowadays have the trend to be lightly doped for improving electrical characteristics. In the section, we concentrate on the quantum barrier field, V_B. Use the property of a barrier potential, shown as [51]

$$e\nabla V_B(x) = B(1,0,0)^T\delta(y), \tag{4.53}$$

where B is the barrier height and y refers to growth direction, i.e. along depth. Fourier transforming of Eq. (4.53) becomes

$$e\widehat{\nabla V_B}(\xi) = \frac{B}{2\pi}\delta(\xi_x)\delta(\xi_z)(1,0,0)^T, \tag{4.54}$$

Combining Eq. (4.51), Eq. (4.53) and Eq. (4.54) to give

$$e\nabla V_B^{eff}(y,p) = \frac{B}{2\pi}(1,0,0)^T\int_R exp(-\beta\frac{\hbar^2|\xi_y|^2}{8m^*})\frac{2m^*}{\beta\hbar p_y\cdot\xi_y}sinh(\frac{\beta\hbar p_y\cdot\xi_y}{2m^*})exp(i\xi_y\cdot y)d\xi_y. \tag{4.55}$$

After solving partial differential equation Eq. (4.55), we can successfully obtain the ”Quantum Barrier Field” corrections. Basically, the thermodynamic effective potential is particle-based simulation, i.e. Monte Carlo method [51], because the distribution of momentum along growth direction has to be known.

Chapter 5

Application to Nanoscale MOS Structures

Among the quantum correction models described above, Van Dort model is the most inaccurate, thermodynamic effective potential is a particle based model (Monte Carlo simulation), and modified density-gradient model, doesn't have so much benefits in the low-dimensional simulation. So in this chapter, we used the Hänsch, Li, MLDA, effective potential, and density-gradient models for applications on Nanoscale MOS structures. The properties of models described above are shown in Fig. 5.1.

Model	**Expression**	**Implementation**
Van Dort	explicit	- simple to implement
Li	explicit	-simple to implement -difficult extraction pf parameters
Hänsch	explicit	- Simple to implement
MLDA	explicit	- involves an extra integration
EP	explicit	- a convenient way to produce a first-order result
TEP	1 PDEs to be solved	- particle based simulation
DG	1 PDE to be solved	- has numerical convergence troubles - needs special setting on boundary conditions
Modified DG	1 PDE to be solved	- needs special setting on boundary conditions

Figure 5.1: Properties of the quantum correction models for simulation.

5.1 Effective Mass Calculation for Quantum Correction Models

The effective mass included in the quantum corrected models are often treated as fitting parameters, which are compared with Schr$\ddot{o}$dinger-Poisson results to find the optimal value. One of the disadvantage of quantum correction models is that this fitting parameters change by case. Different values are chosen in varied physical conditions, for example, gate voltage, gate oxide thickness, channel doping concentration and so on. A single-gate MOSFET is shown in Fig. 5.2 and the red cut-line in the center of a 1-D MOS capacitor, is the simulation domain. Fig. 5.3 to Fig. 5.6 show the proper effective potential, m$_k$ versus varied surface electric field in the case of single-gate MOS structure for H$\ddot{a}$nsch, MLDA, EP and DG models. The verified ranges of physical settings are $1e15$ to $5e18cm^{-3}$ for substrate doping, 1 to 5 nm for oxide thickness and 0.5 to 2 for gate voltage. The surface electric field integrate all the physical parameters mentioned above into consideration. We can see that each different surface electric filed corresponds to an unique m$_k$. We note that effective mass m_n^* is originally defined as

$$\frac{1}{m_n^*} = \frac{1}{\hbar^2}\frac{d^2\epsilon}{dk^2}, \tag{5.1}$$

where ϵ is band energy. However, the effective masses we use here are not derived from Eq. (5.1). They are seen to be pure fitting parameters, thus, the value of the fitting parameters

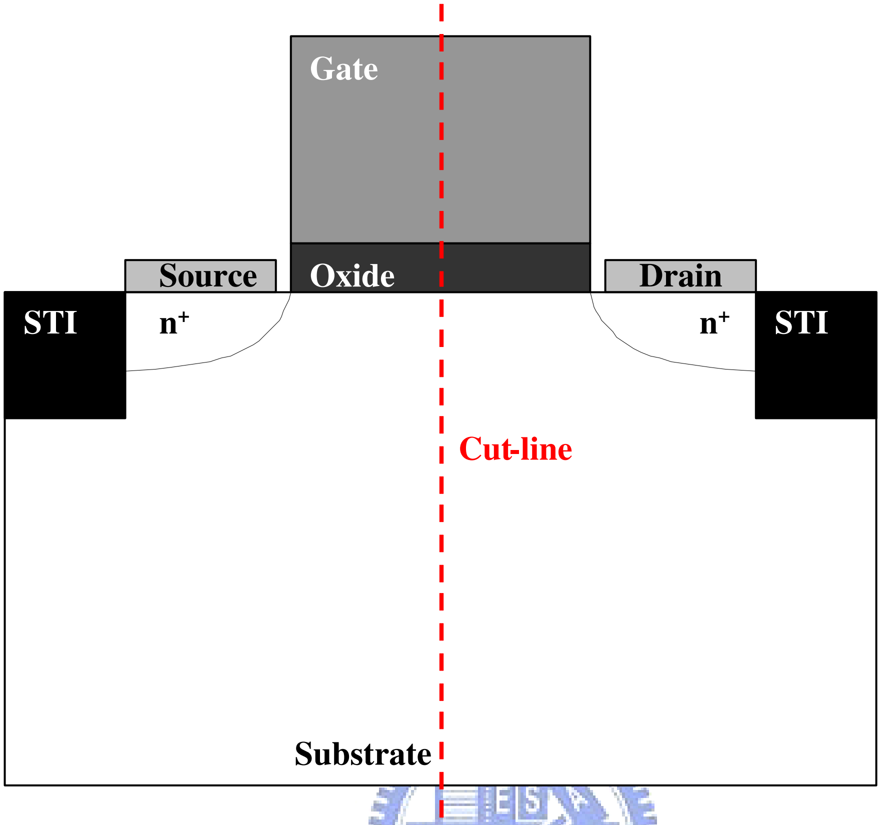

Figure 5.2: Single-gate MOS structure, where the red-dashed cut-line is the simulation domain.

if they are larger or smaller than one don't have much physical meanings [53].

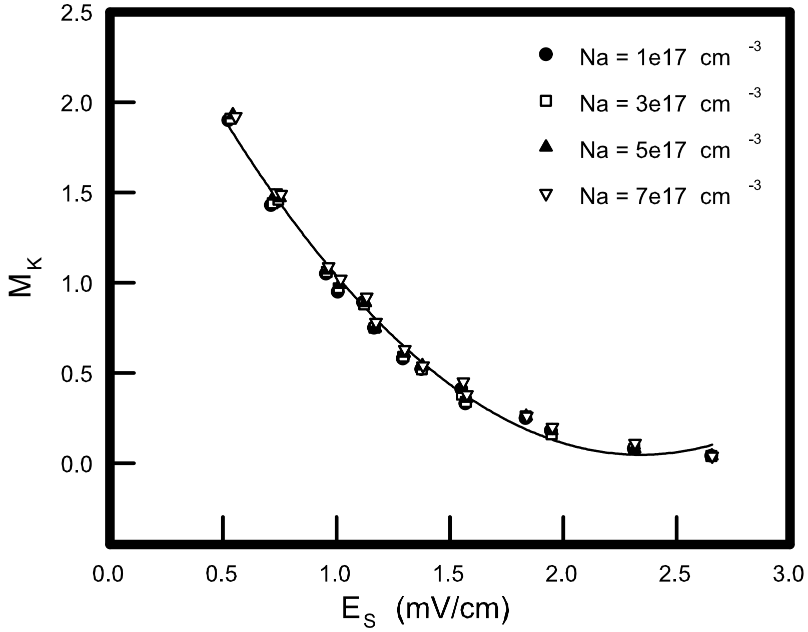

Figure 5.3: Effective mass, M_k, versus surface electric field, E_s, for Hänsch model by different substrate doping.

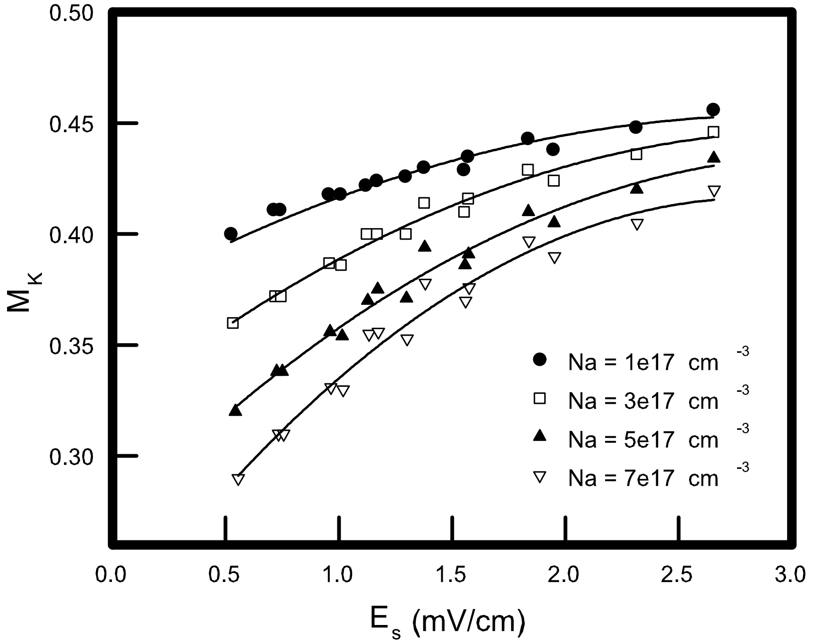

Figure 5.4: Effective mass, M_k, versus surface electric field, E_s, for MLDA model by different substrate doping.

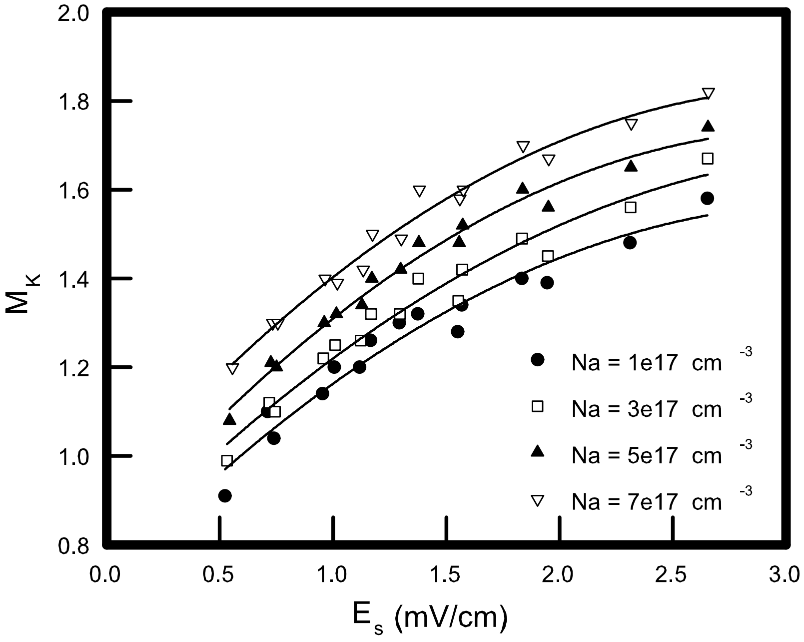

Figure 5.5: Effective mass, M_k, versus surface electric field, E_s, for EP model by different substrate doping.

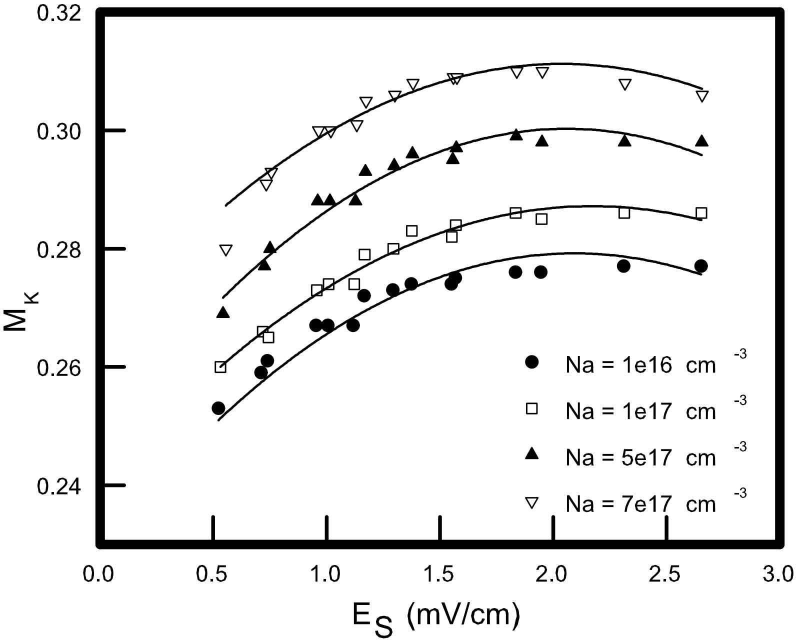

Figure 5.6: Effective mass, M_k, versus surface electric field, E_s, for DG model by different substrate doping.

5.2 Computation of Electron Density of MOS Structure under Inversion Condition

Classical and quantum simulation results are studied and then we compare the H$\ddot{a}$nsch, MLDA, effective potential, and density-gradient models with each other on a MOS capacitor.

5.2.1 Single-Gate MOS Structure

Fig. 5.7 shows the Schr$\ddot{o}$dinger-Poisson and classical results in different gate oxide thickness. The gate voltage is 1 V and substrate doping is $1e18cm^{-3}$. We can observe that the average displacement of the electric density in quantum case is far from the interface of Si/SiO$_2$, which means no electrons are at the surface because of a finite size of electron. And the peak value is lower than classical results. By increasing of gate oxide thickness, the induced electrons in the inversion layer decrease rapidly because the ability of gate control is reduced. We compare the H$\ddot{a}$nsch, MLDA, EP and DG models with each other on the single-gate MOS structure. Density-gradient model fits the Schr$\ddot{o}$dinger-Poisson results best, the second is MLDA model. H$\ddot{a}$nsch model has a wrong average displacement position and electron density. Effective potential model overestimates the peak value of

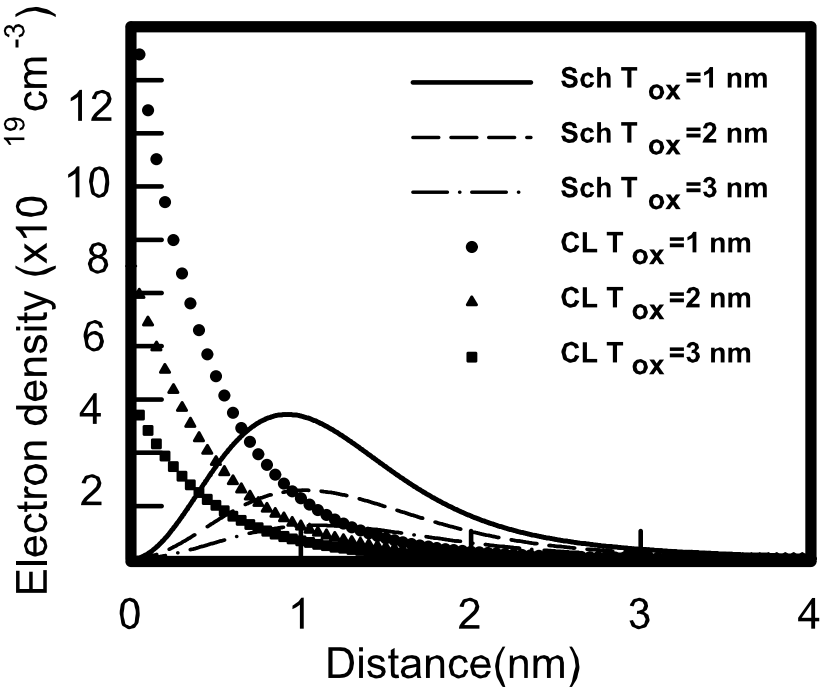

Figure 5.7: Comparison of electron density between Schrödinger and classical results for single-gate MOS structure, where gate voltage is 1 V and channel doping is $1e18cm^{-3}$ [40].

electron density and a further distance away from gate oxide.

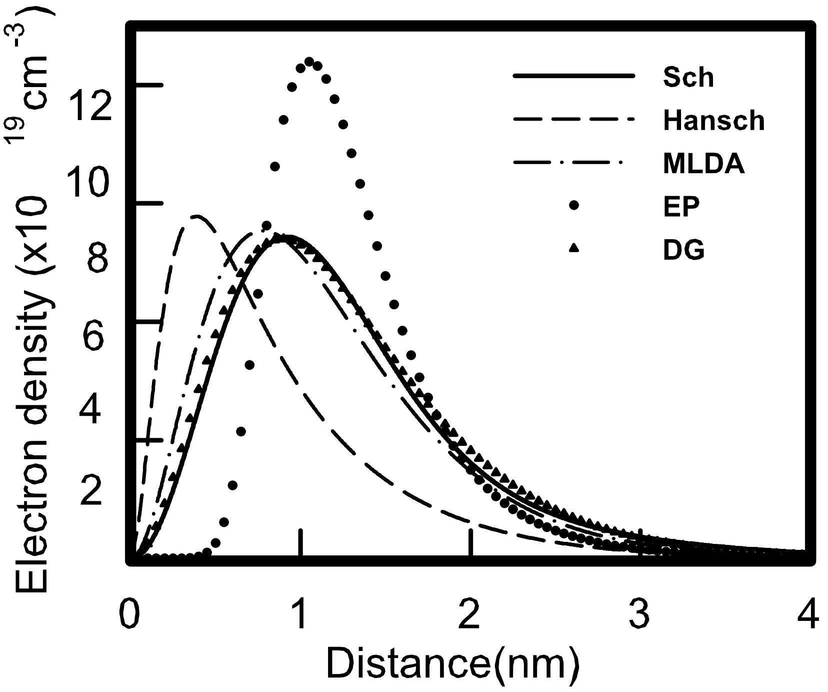

Figure 5.8: Comparison of electron density for Schrödinger results with verified quantum models for single-gate MOS structure, where gate oxide thickness is 1 nm, gate voltage is 1 V and channel doping is $1e18cm^{-3}$. "Sch" means solutions of Schrödinger equation and "CL" means classical results.

5.2.2 Double-Gate MOS Structure

The same models are used for double-gate MOS structure investigation. Fig. 5.9 shows a double-gate MOSFET structure. The red cut-line denotes the simulation domain, where top gate (gate 1) voltage is the same as bottom gate (gate 2) as 1 V, silicon body thickness is 15 nm and channel doping is $1e17cm^{-3}$. The same physical phenomenons are observed again, i.e. the electric density distribution in quantum case is far from the interface of Si/SiO$_2$ and the peak value is lower than classical results. comparing these models on double-gate MOS capacitor with each other, density-gradient model fits the Schr$\ddot{o}$dinger-Poisson results very well. H$\ddot{a}$nsch and MLDA models have rise trends of electron density in the center of silicon body, but there are no physical meanings. Effective potential model overestimates the peak value of electron density and a further distance away from gate oxide [21].

The conclusions of the quantum models are listed in Fig. 5.12. The H$\ddot{a}$nsh model has the most sensitive effective mass, m_k. Effective potential model results in a overestimated solution and peak location is further setback from the material interfaces. Density-gradient model is the most accurate when applied in the single-gate and double-gate cases. We note that H$\ddot{a}$nsh and MLDA models lead to a raise of electron density in the center of silicon body which has no physical meanings when applied in double-gate MOSFETs [21].

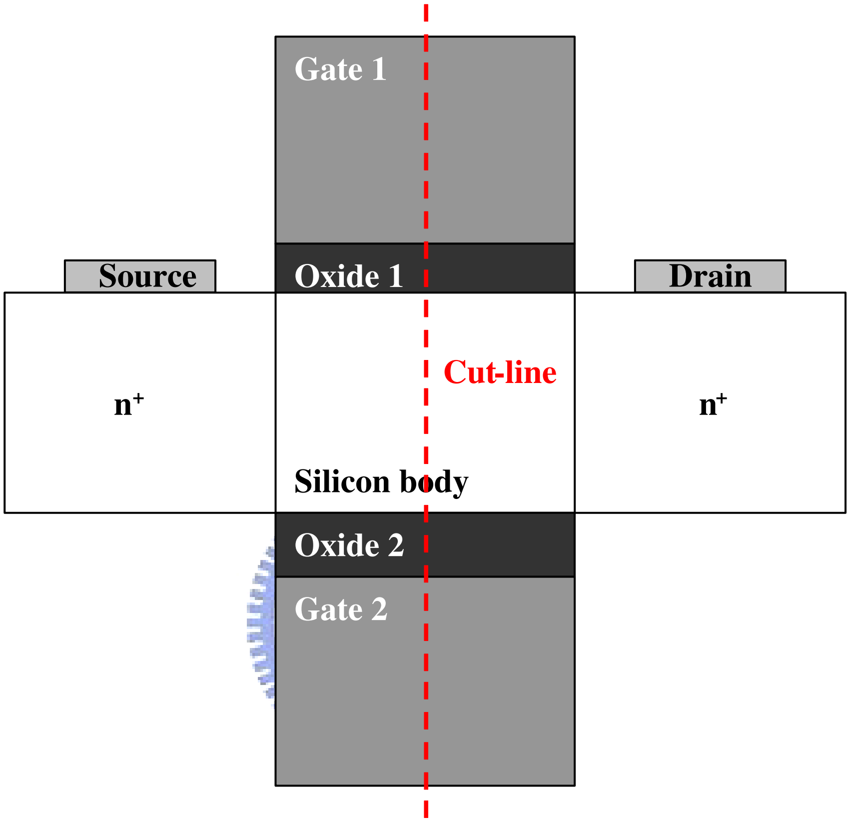

Figure 5.9: Double-gate MOS structure, where the red-dashed cut-line is the simulation domain [21].

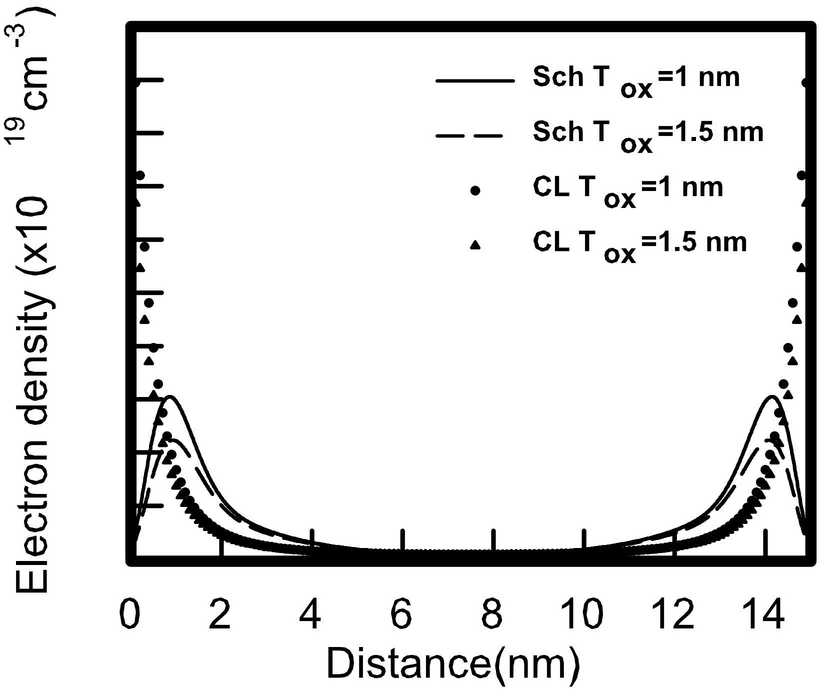

Figure 5.10: Comparison of electron density between Schrödinger and classical results for double-gate MOS structure, where gate oxide thickness is 1 nm, top gate voltage is equal to top gate voltage as 1 V and silicon body thickness is 15 nm [21].

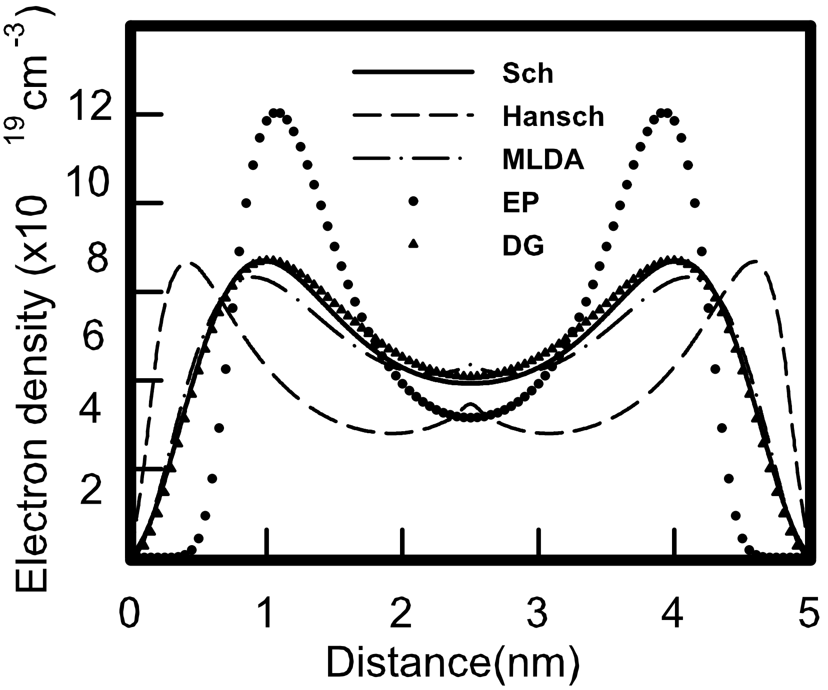

Figure 5.11: Comparison of electron density for Schrödinger results with verified quantum models for double-gate MOS structure, where gate oxide thickness is 1 nm, top gate voltage is equal to top gate voltage as 1 V and channel doping is $1e17cm^{-3}$.

Model	**Single-gate MOS Results**	**Double-gate MOS Results**
Hänsch	- solution is the most sensitive to m_k	-solution is the most sensitive to $m_{k;}$ -raise of electron density in the center of silicon body.
MLDA	- better than Hänsch model	-better than Hänsch model; -raise of electron density in the center of silicon body.
Li	- solution is close to that of SP equations	-solution is close to that of SP equations
EP	- solution is overestimated and peak location is further setback from the material interfaces	- solution is overestimated and peak location is further setback from the material interfaces
DG	- solution is close to that of SP equations	- solution is close to that of SP equations

Figure 5.12: Comparison of quantum correction models applied on single-gate and double-gate MOSFETs.

5.3 Terminal Characteristics Simulation Using Quantum Correction Models

Although effective potential model overestimate the peak quantity of electron density and a further distance away from gate oxide, it has the advantages of fast and easy implantation in simulation tools. In the single-gate MOS capacitor, Fig. 5.13 shows the ratio of $< x >_{EP}$ over $< x >_{Sch}$, where $< x >$ means the average displacement of electron density defined as

$$\frac{\int_0^\infty xn(x)dx}{\int_0^\infty n(x)dx}. \tag{5.2}$$

We find that effective potential model is more accurate in high gate voltage than low one. By Fig. 5.8, Fig. 5.11 and Fig. 5.13, we conclude that effective potential leads to a shift electron distribution. However, these inaccuracy won't result in a wrong trend of C-V results compared with Schr$\ddot{o}$dinger and measurement data shown is Fig. 5.14, where the oxide thickness is 1.6 nm and frequency is fixed at 100 KHz. The measurement data show a descended trend of capacitance at a high gate voltage because gate tunnelling current becomes obvious. The simulation results can't observe the phenomenon because the gate leakage model is neglected [41]. Finally, we perform the 2-D quantum correction with effective potential model. Fig. 5.15 shows the electron distribution in a double-gate silicon body of top gate voltage is the same as the bottom gate of 1 V and drain voltage is 0.5 V.

The peak values of electron density appear near the boundary of gates and drain because the electric field is modified to increase by additional drain voltage. Fig 5.16 shows the diagram of drain current versus gate voltage in the case of top gate voltage is the same as the bottom gate of 0.7 V, gate length is 20 nm, silicon body thickness is 10 nm and gate oxide thickness is 2 nm. By the Fig. 5.16, we take use of the improved Hänsch's model [21]. The model is shown as

$$n_Q(x) = a_0 n_{CL}(x) \cdot (1 - exp[-a_1 \xi^2 (1 - \frac{1}{2}(\frac{\xi}{\xi_0})^2) - a_2 \xi^3]), \tag{5.3}$$

where $n_{CL}(x)$ is the classical electron density solved with the Poisson equation, $\xi = x/\lambda_{th}$ and λ_{th} is the thermal wavelength. For the double-gate case, $\xi_0 = T_{si}/2\lambda_{th}$, where T_{si} is the thickness of silicon body. a_0, a_1 and a_2 are optimized and calibrated with the Schrödinger-Poisson solutions by optimization theory. We obtain the result of a 20 nm double-gate MOSFET that drain current considering quantum effects is reduced when compared with that using classical transport equations [21].

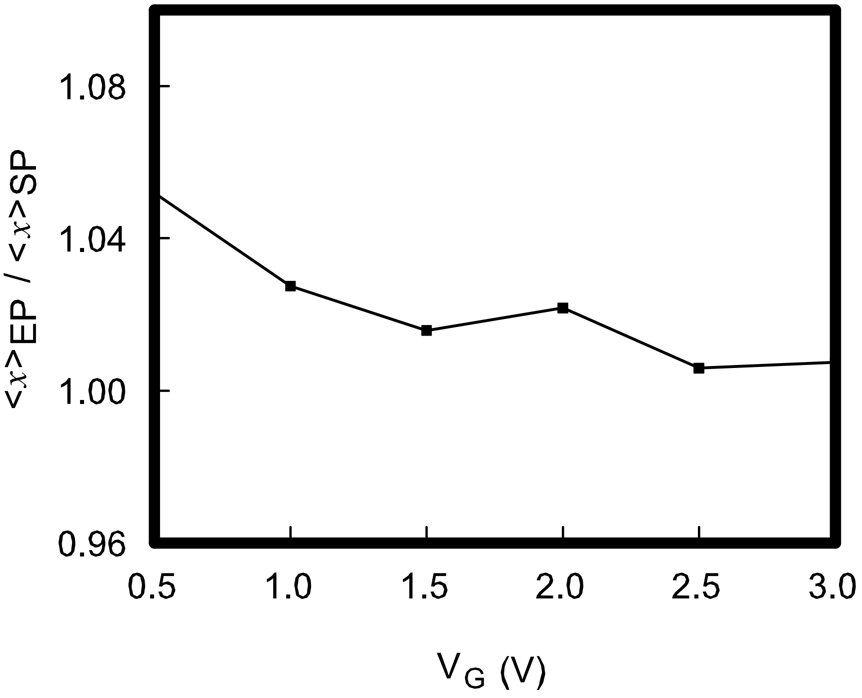

Figure 5.13: Plot of ratio of $< x >_{Sch}$ over $< x >_{EP}$ versus verified gate voltage. The substrate doping is assumed to be uniform distribution of $1e18cm^{-3}$.

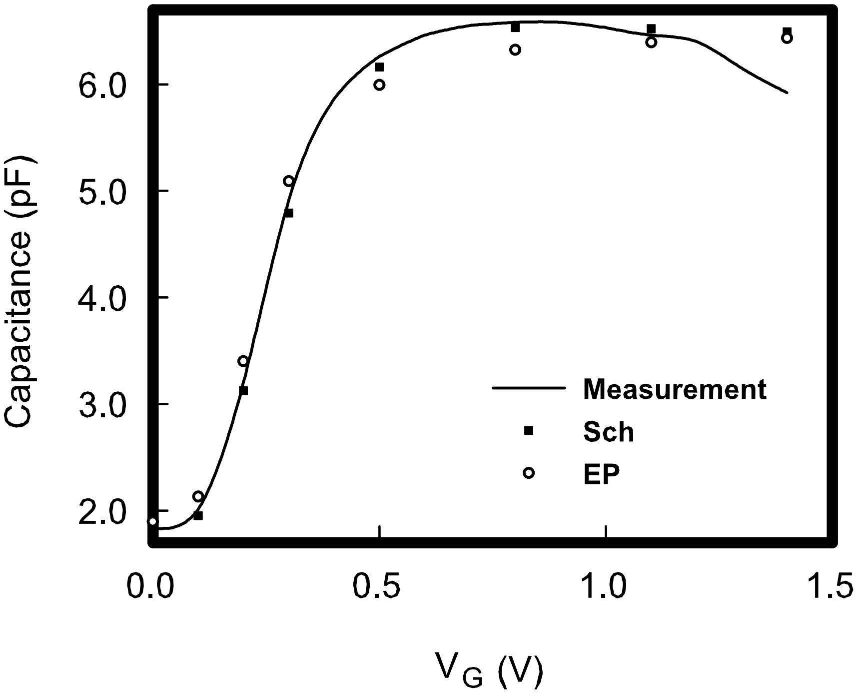

Figure 5.14: Comparison of capacitance versus gate voltage between measurement data, Schrödinger and effective potential results.

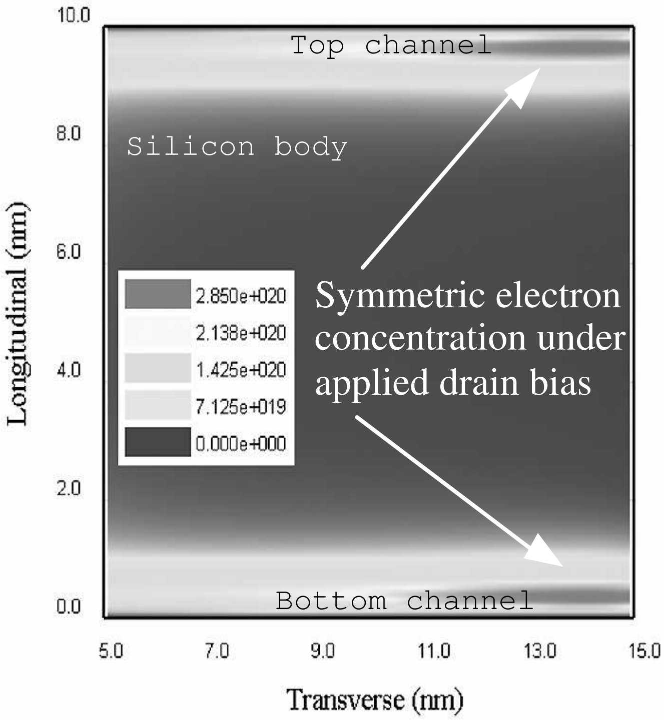

Figure 5.15: 2-D electron distribution in a double-gate MOSFET biased at top gate voltage is the same as the bottom gate of 1 V and drain voltage is 0.5 V [21].

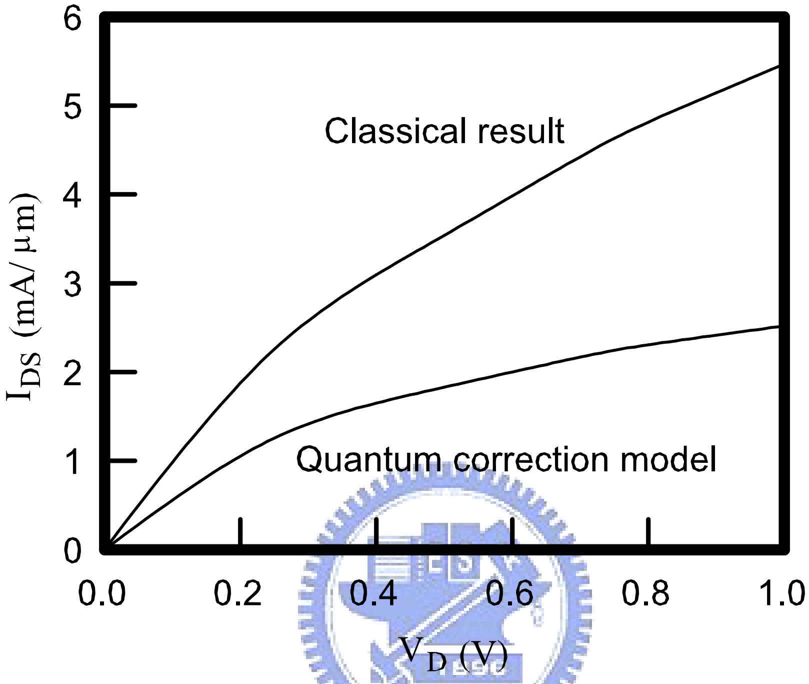

Figure 5.16: Comparison of drain current versus gate voltage calculated by classical and quantum corrected transport model, where we adopt Li's model. Top gate voltage is the same as the bottom gate of 0.7 V, gate length is 20 nm, silicon body thickness is 10 nm and gate oxide thickness is 2 nm [21].

Chapter 6

Conclusions

In this thesis, explicit and implicit quantum correction models are introduced completely. We compare these models with each other in terms of theoretical and numerical viewpoints respectively. Effective masses for varied quantum correction models used in optional physical settings are extracted.

6.1 Summary

Schrödinger-Poisson model is the most accurate way for calculating quantum effects. However, it is time-consuming and difficult to solve because of eigenvalue problem. So quantum correction models are alternative way to consider quantum effects in semiconductor simulation. In this work, explicit and implicit quantum correction models have been introduced completely. There are Van Dort's, Hänsch's, Li's, MLDA and EP models in explicit forms; DG, modified DG, thermodynamic EP models are implicit form. We compare these models with each other to determine the properties and accuracy. To find the relationship between the effective mass which is treated as fitting parameters in the models with varied physical settings is benefit for industry applications, especially the explicit models, they are simple to be implanted in the simulator. In application, C-V characteristics of a MOS structure and IV curves of a 20 nm double-gate MOSFET have been numerically investigated in the work.

6.2 Future Work

Listed below are a few topics which require further investigation:

1. EP model has the properties of fast calculation and easy implantation into simulation tools. Therefore, improvement of the model, for example, thermodynamic approximation, is a potential way to keep accuracy and fast speed at the same time. However, the momentum distribution the thermodynamic effective potential model needs to know is extracted by Monte Carlo simulation. The particle-based method takes

too much time. Therefore, derivation of analytical momentum distribution along the growth direction will make the thermodynamic effective potential model more adaptable;

2. Extend the quantum correction models to more advanced device structures, such as silicon-on-insulator (SOI), ultra-thin-barrier (UTB) SOI, tri-gate MOSFETs and surrounding-gate MOSFETs;

3. Extend the quantum correction models by considering strain effect of lattice. Not only properties of electrons, properties of holes become very important in that case.

Bibliography

[1] J. R. Schrieffer, ”Semiconductor Surface Physics,” University of Pennsylvania press, Philadelphia 1957.

[2] F. Stern and W. E. Howard, ”Properties of Semiconductor Surface Inversion Layers in the Electric Quantum Limit,” Physical Review, Vol. 163, No. 3, 1967, pp. 816-834.

[3] F. Stern, ”Self-Consistent Results for n-Type Si Inversion Layers,” Physical Review B, Vol. 5, No. 12, 1972, pp. 4891-4899.

[4] M. J. Van Dort, P. H. Woerlee and A. J. Walker, ”A Simple Model for Quantization Effecs in Heavily-Doped Silicon MOSFETs at Inversion Conditions,” Solid-State Electrnics, Vol. 37, No. 3, 1994, pp. 411-414.

[5] T. W. Tang, X. Wang and Y. Li, ”PDiscretization Scheme for the Dnesity-Gradient Equations and Effect of Boundary Conditions,” Journal of Computational Electronics, Vol. 1, No. 3, 2002, pp. 389-393.

[6] M. G. Ancona, ”Equations of States for Silicon Inversion Layers,” IEEE Trans. Electron Devices, Vol. 47, 2000, pp. 1449-1456.

[7] Y. Li, T. W. Tang and X. Wang, ”Modeling of Quantum Effects for Ultrathin Oxide MOS Structures with an Effective Potential,” IEEE Trans. Nanotechnology, Vol. 163, No. 4, 2002, pp. 238-242.

[8] S. M. Ramey and D. K. Ferry, ”Implementation of Surface Roughness Scattering in Monte Carlo Modeling of Thin SOI MOSFETs Using the Effective Potetial,” IEEE Trans. Nanotechnology, Vol. 2, 2003, pp. 110-114.

[9] S. M. Ramey and D. K. Ferry, ”Threshold Voltage Calculation in Ultrathin-Film SOI MOSFETs Using the Effective Potential,” IEEE Trans. Nanotechnology, Vol. 2, 2003, pp. 121-125.

[10] L. Shifren, R. Akis and D. K. Ferry, ”Correspondence Between Quantum and Classical Motion: Comparing Bohmian Mechanics with a Smoothed Effective Potential Approach,” Physical Letters A, Vol. 274, 2000, pp. 75-83.

[11] W. Hänsch, T. Vogelsang, R. Kircher and M. Orlowski, Solid-State Electronics, Vol. 32, 1989, pp. 839.

[12] J. R. Hauser and M. A. Littlejohn, ”Approximation for Accumulation and Inversion Space-Charge Layers in Semiconductors,” Solid-State Electronics, Vol. 11, 1968, pp. 667-674.

[13] M. G. Ancona and H. F. Tiersten, ”Fully Macroscopic Description of Bounded Semiconducors with an Application to the Si-SiO2 Interface,” Physical Review B, Vol. 22, No. 12, 1980, pp. 6104-6119.

[14] M. G. Ancona and H. F. Tiersten, ”Fully Macroscopic Description of Electrical Consuction in Metal-Insulator-Semiconductor Structures,” Physical Review B, Vol. 27, No. 12, 1983, pp. 7018-7045.

[15] M. G. Ancona and H. F. Tiersten, ”Macroscopic Physics of the Silicon Inversion Layer,” Physical Review B, Vol. 35, 1987, pp. 7959-7965.

[16] Y. Li and Y. Y. Cho ”Intelligent BSIM4 Model Parameter Extraction for Sub-100 nm MOSFET Era,” Japanese Journal of Applied Physics, Vol. 43, No.4B , 2004, pp. 1717-1722.

[17] G. Paasch and H. Ubesee, ”A Modified Local Density Approximation,” Physical Static Solutions (b), Vol. 113, 1982, pp. 165-178.

[18] A. Asenov, J. R. Watling, A. R. Brown and D. K. Ferry, ”The Use of Quantum Potentials for Confinement and Tunneling in Semiconductor Devices,” Journal of Computational Electronics, Vol. 1, 2002, pp. 503-513.

[19] D. K. Ferry, ”Effective Potential and the Onset of Quantization in Ultrasmall MOSFETs”, Superlattices and Microstructures, Vol. 28, 2000, pp. 419-423.

[20] T. W. Tang and B. Wu, ”Quantum Correction for the Monte Carlo Simulation via the Effective Conduction-Band Edge Equation,” Semiconductor Science and Technology, Vol. 19, 2004, pp. 54-60.

[21] Y. Li and S. M. Yu, ”A Unified Quantum Correction Model for Nanoscale Single- and Double-Gate MOSFETs Under Inversion Conditions,” Nanotechnology, Vol. 15, 2004, pp. 1009-1016.

[22] C. Ringhofer, C. L. Garder and D. Vasileska, ”Effective Potentials and Quantum Fluid Models: A Thermodynamic Approach,” Inter. J. on High Speed Electronics and Systems, Vol. 13, 2003, pp. 771-803.

[23] W. Fichtner, ”PSemiconductor Device Simulation,” IEEE Trans. Electron Devices, Vol. 30, No. 9, 1983, pp. 1018-1041.

[24] D. J. Griffiths, Introduction to Electrodynamics. 3rd edition, Prentice-Hall, London, 1999.

[25] D. K. Cheng, Field and Wave Electromagnetics, 2nd edition, Addison-Wesley, New York, 1989.

[26] C. M. Snowden, Introduction to Semiconductor Device Modelling, World Scientific, Singapore, 1986.

[27] R. R. Schaller, ”Moore’s Law: Past, Present and Future,” IEEE Spectrum, Vol. 34, No. 6, 1997, pp. 52-59.

[28] C. Cercignani, The Boltzmann Equation and Its Applications, Springer-Verlag, New York, 1988.

[29] S. Succi, The Lattice Boltzmann Equation for Fluid Dynamics and Beyond, Oxford University Press, New York, 2001.

[30] K. Blϕtekjaer, ”Transport Equations for Electrons in Two-Valley Semiconductors,” IEEE Trans. Electron Devices, Vol. 17, No. 1, 1970, pp. 38-47.

[31] R. Stratton, ”Diffusion of Hot and Cold Electrons in Semiconductor Barriers,” Physical Review, Vol. 126, No. 6, 1962, pp. 2002-2014.

[32] L. P. Kadanoff and P. C. Martin, ”Hydrodynamic Equations and Conclation Functions,” Annal of Physics, Vol. 281, No. 1, 2000, pp. 800-852.

[33] G. Wachutka, ”An Extended Thermodynamic Model for the Simultaneous Simulation of the Thermal and Electrical Behavior of Semiconductor Devices,” Proceedings of the Sixth International NASECODE Conference, 1989, pp. 409-414.

[34] C. Kittel and H. Kroemer, Thermal Physics, 2nd, W. H. Freeman and Company, Nwe York, 1980.

[35] N. B. Addallah, P. Degond and S. Genieys, ”An Energy-Transport Model for Semiconductors Derived From the Boltzmann Equation,” Jounal of Statistical Physics, Vol. 84, No. 1-2, 1996, pp. 205-231.

[36] W. Hänsch, The Drift Diffusion Equation and Its Applications in MOSFET Modeling, Springer-Verlag, New York, 1991.

[37] F. L. Yang, D. H. Lee, H. Y. Chen, C. Y. Chang, S. D. Liu, C. C. Huang, T. X. Chung, H. W. Chen, C. C. Huang, T. H. Liu, C. C. Wu, C. C. Chen, S. C. Chen, Y. T. Chen, Y. H. Chen, C. J. Chen, B. W. Chan, P. F. Hsu, J. H. Shieh, H. J. Tao, Y. C. Yeo, Y. C. Yeo, Y. Li, J. W. Lee, P. Chen, M. S. Liang and C. Hu, ”5nm Gate Nanowire FinFET,” VLSI Technology Tech. Symp. Dig., 2004, pp. 193-197.

[38] N. Zettili, Quantum Mechanics, John Wiley and Sons, Chichester, 2001.

[39] J. A. Lòpez-villanueva, I. Melchor, F. Gámiz, J. Banqueri and J. A. Jinénez-Tejada, ”A Model for the Quantized Accumulation Layer in Metal-Insulator-Semiconductor Structures,” Solid-State Electronics, Vol. 38, No. 1, 1995, pp. 203-209.

[40] X. Wang, ”Quantum Correction to the Charge Density Distribution in Inversion Layers,” Master Thesis of University of Massachusetts Amherst, MA, 2001.

[41] S. M. Sze, Physics of Semiconductor Devices, 2nd edition, Wiley-Interscience, New York, 1981.

[42] A. S. Spinelli, A. Benvenuti, ”Self-consistent 2-D Model for Quantum Effects in n-MOS Transistors,” IEEE Trans. Electron Devices, Vol. 45, No. 6, 1998, pp. 1342-1349.

[43] W. Magnus and W. Schoenmaker, Quantum Transport in Submicron Devices, Springer, New York, 2003.

[44] D. Bohm, ”A Suggested Interpretation of the Quantum Theory in Terms of ”Hidden” Variables,” Physical Review, Vol. 85, No. 2, 1952, pp. 166-179.

[45] S. S. Ahmed, C. Ringhofer and D. Vasileska, ”An Effective Potential Approach to Modeling 25 nm MOSFET Devices,” Journal of Computational Electronics, Vol. 2, 2003, pp. 113-117.

[46] E. Wigner, ”On the Quantum Correction for Thermodynamic Equilibrium,” Physical Review, Vol. 40, 1932, pp. 749-759.

[47] L. Shifren and D. K. Ferry, ”Partical Monte Carlo Simulation of Wigner Function Tunneling,” Physics Letters A, Vol. 285, 2001, pp. 217-221.

[48] C. L. Gardner and C. Ringhofer, ”Smooth Quantum Potential for the Hydrodynamic Model,” Physical Review, Vol. E53, 1996, pp. 157-167.

[49] C. Gardner and C. Ringhofer, ”Approxamation of Thermal Equilibrium for Quantum Gases with Discontinuous Potentials and Application to Semiconductor Devices,” SIAM Journal on Applied Mathematics, Vol. 58, 1998, pp. 780-805.

[50] P Feynman and H. Kleinert, ”Effective Clasical Partition Functions,” Physical Review A, Vol. 34, 1986, pp. 5080-5084.

[51] S. S. Ahmed, ”Modeling Quantum and Qoulomb Effects in Nanoscale Devices,” Ph.D. Dissertation of Arizona State University, Arizona, 2005.

[52] L. Shifren and D. K. Ferry, ”Particle Monte Carlo Simulation of Wigner Function Tunneling,” Physics Letters A, Vol. 285, 2001, pp. 217-221.

[53] S. A. Mujtaba, ”Advanced Mobility Models for Design and Simulation of Deep Submicrometer MOSFETs,” Ph.D. Dissertation of Stanford University, CA, 1995.

VITA

Name: Wei-Hsin Chen, 陳煒昕

Permanent address: 2F., No. 28, Lane 97, Sec. 1, Sinsheng S. Rd.,
Taipei City 106, Taiwan

Degree and date to be conferred: Master of Science, July, 2006

Date of birth: August 27th, 1982

Place of birth: Taipei, Taiwan

Collegiate institutions attended	Degree	Date of graduate
Department of Electrophysics National Chaio Tung University, Hsinchu, Taiwan	BS	June, 2004
Department of Electrophysics National Chaio Tung University, Hsinchu, Taiwan	MS	July, 2006

Master thesis title: Modeling of Quantum Mechanical Effects for Nanoscale MOS Devices with Correction Theory

Publication List:

1. Yiming Li and **Wei-Hsin Chen**, “Numerical Simulation of Electrical Characteristics for Nanoscale MOSFETs with Si/GaAs Channel Film,” Journal of Computational Electronics, vol. 5, 2006, pp. 255-258.

2. Yiming Li and **Wei-Hsin Chen**, “Simulation of Nanoscale Round-Top-Gate Bulk FinFETs with Optimal Geometry Aspect Ratio,” The 6th IEEE Conference on Nanotechnology (IEEE- NANO 2006), Cincinnati, Ohio, U.S.A., July 16-20, 2006, S09P12.

3. Yiming Li and **Wei-Hsin Chen**, "Electrical Characteristics on Ellipse-Shaped-Surrounding-Gate Nanowire FinFETs," The 2006 IEEE Silicon Nanoelectronics Workshop (IEEE SNW 2006), Honolulu, Hawaii, U.S.A., June 11-12, 2006, pp. 181-182.

4. Yiming Li and **Wei-Hsin Chen**, "Numerical Simulation of Electrical Characteristics on Uniaxial Strained Bulk and SOI FinFETs," The 11th IEEE International Workshop on Computational Electronics (IEEE IWCE-11), Vienna, Austria, May 25-27, 2006, pp. 71-72.

5. Yiming Li and **Wei-Hsin Chen**, "Effect of Fin Angle on Electrical Characteristics of Nanoscale Bulk FinFETs," The 2006 NSTI Nanotechnology Conference and Trade Show (Nanotech 2006), vol. 3, Boston, Massachusetts, U.S.A., May 7-11, 2006, pp. 20-23.